ACS Photonics

pubs.acs.org/journal/apchd5

Perspective

Silicon Carbide Photonics Bridging Quantum Technology

Stefania Castelletto,* Alberto Peruzzo, Cristian Bonato, Brett C. Johnson, Marina Radulaski, Haiyan Ou, Florian Kaiser, and Joerg Wrachtrup

Cite This: *ACS Photonics* 2022, 9, 1434−1457

Read Online

ACCESS | Metrics & More | Article Recommendations

ABSTRACT: In the last two decades, bulk, homoepitaxial, and heteroepitaxial growth of silicon carbide (SiC) has witnessed many advances, giving rise to electronic devices widely used in high-power and high-frequency applications. Recent research has revealed that SiC also exhibits unique optical properties that can be utilized for novel photonic devices. SiC is a transparent material from the UV to the infrared, possess nonlinear optical properties from the visible to the mid-infrared and it is a meta-material in the mid-infrared range. SiC fluorescence due to color centers can be associated with single photon emitters and can be used as spin qubits for quantum computation and communication networks and quantum sensing. This unique combination of excellent electronic, photonic and spintronic properties has prompted research to develop novel devices and sensors in the quantum technology domain. In this perspective, we highlight progress, current trends and prospects of SiC science and technology underpinning the development of classical and quantum photonic devices. Specifically, we lay out the main steps recently undertaken to achieve high quality photonic components, and outline some of the current challenges SiC faces to establish its relevance as a viable photonic technology. We will also focus on its unique potential to bridge the gap between classical and quantum photonics, and to technologically advance quantum sensing applications. We will finally provide an outlook on possible alternative applications where photonics, electronics, and spintronics could merge.

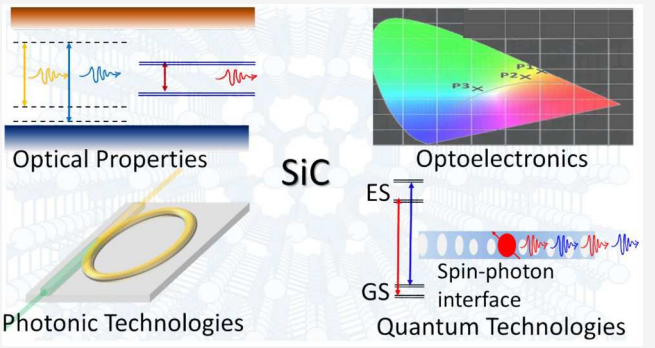

KEYWORDS: *photoluminescence, nonlinear optics, point defects in the bandgap, single photon source, quantum sensing, quantum nanophotonics*

INTRODUCTION

This Perspective summarizes the properties of silicon carbide (SiC), a material that uniquely enables the integration of electronic, spintronic, and photonic functionalities within the same platform.

SiC is a wide bandgap compound semiconductor with extensive industrial applications. While silicon is the material currently most used in microelectronics, advances in the material quality, and the fabrication processes are pushing SiC to surpass silicon for high power and high temperature applications[1−3] crucial for the future economy of zero-emission electric vehicles.[4]

Photonics is currently less established in SiC than in a variety of competing technologies and material platforms. In the emerging area of photonic integrated circuits (PICs), consisting of semiconductor wafers with optically active integrated photonic devices, the first commercial PICs were based on group III−V indium phosphide (InP) semiconductor wafer substrates[5] followed by the most widely used silicon. In addition, there are many other contenders, such as Si_3N_4, AlN, diamond, and lithium niobate (LN). Despite this, SiC is a very appealing platform for photonics, with optical transparency in a large spectral region and its high second and third order nonlinear optical properties make it an attractive material for integrated architectures. Remarkably, despite its indirect bandgap, SiC was actually the first material to be used as a commercial light emitting diode (LED), holding a unique place in history for its capabilities in the generation, detection, and manipulation of light.

In the past decade, SiC has attracted the interest of the quantum technology community, due to the availability of a variety of point defects that can act as quantum emitters[6] with controllable electronic spins.[7,8] Importantly, spin coherence for these systems has been shown to be comparable or even superior to more established quantum emitters such as the nitrogen-vacancy (NV) center in diamond.[9−11] Recently, simulations[12]

Received: November 18, 2021
Revised: March 31, 2022
Accepted: March 31, 2022
Published: April 18, 2022

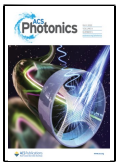

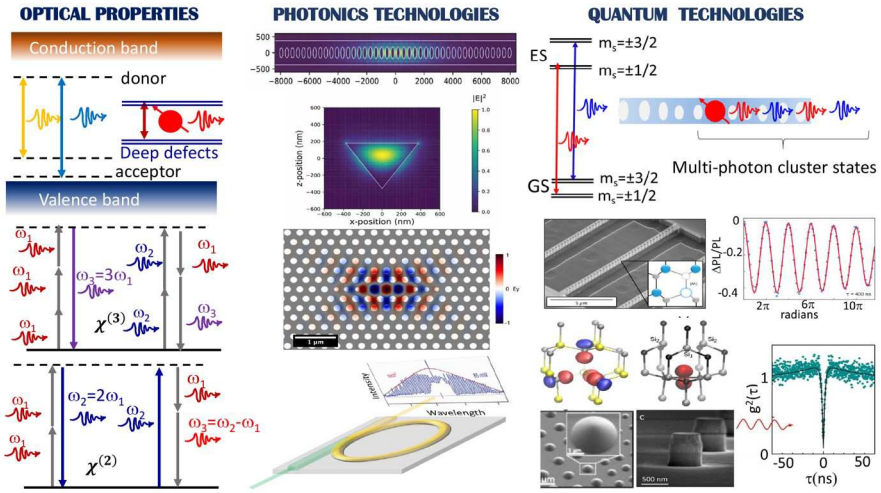

Figure 1. Overview of SiC optical properties and photonic and quantum technologies discussed in this paper. Optical properties: From top to bottom: fluorescence emission due to donor and acceptor pairs or deep color centers within the bandgap. Nonlinear harmonic generation (third harmonic and four wave mixing based on $\chi^{(3)}$, and second harmonic and SPDC based on $\chi^{(2)}$). Photonic technologies: 1D triangular cross-section photonic crystal; image reprinted in part with permission from ref 17. Copyright 2021 Institute of Physics under https://creativecommons.org/licenses/by/4.0/. 2D photonic crystal; image reprinted with permission from ref 18. Copyright 2019 American Chemical Society. Microring resonator generating frequency comb spectra. Spectra adapted with permission from ref 19. Copyright 2020 The Optical Society. Quantum Technologies: Using spin control of color center combined with a photonic cavity spin-photon entanglement and multiphoton cluster states can be achieved. Suspended photonic crystal nanobeam, obtained from photoelectrochemical etching in 4H-SiC, provides a platform for increasing the quantum sensing capabilities of integrated divacancy color center. Image reprinted in part with permission from ref 20. Copyright 2020 American Chemical Society. Nanopillars[21] and solid immersion lenses[22] in SiC are used to enhance the emission. Images reprinted in part with permission from ref 21. Copyright 2017 American Chemical Society. Images reprinted in part with permission ref 22. Copyright American Institute of Physics 2020. Orbital structures of color centers such as the $C_{Si}V_C$ and V_{Si} responsible for single photon emission. Images reprinted in part with permission from ref 23. Copyright 2013 Springer Nature. Images reprinted in part with permission from ref 24. Copyright 2019 Springer Nature under the https://creativecommons.org/licenses/by/4.0/.

based on cluster correlation expansion techniques, SiC has emerged to possess the longest coherence times among wide bandgap nonchalcogenides materials.

This unique combination of properties makes SiC an excellent platform to implement quantum photonic integrated chips (QPICs). QPICs will host quantum emitters interfacing single photons with local quantum memories based on a register of individually controllable electronic and nuclear spins. The emitted single photons can be processed on-chip by frequency conversion (enabled by the strong nonlinear optical coefficients), routed through electrically controlled switches, integrated filters, waveguides, directional couplers, and fiber couplers. The preservation of optically encoded quantum states in the circuits requires low losses and high material purity.

Despite the large variety of possible photonic material platforms[13] and the many materials hosting single photon emission[14] or the possibility to generate quantum states of light via nonlinear interaction,[15] SiC is really unique with respect to the possibility to simultaneously integrate all the required photonic, electronic, and spintronic circuitry. In contrast to other optoelectronic platforms such as III−V semiconductors, lithium niobate, Si_3N_4, and AlN, SiC enables the preservation of spin quantum coherence, due to a diluted nuclear spin bath.

Beyond the realm of quantum technologies, the integration of spintronics, photonics, and electronics enabled by SiC can find applications, for example, in extending its neuromorphic computing capacity.[16]

This paper provides an overview of the state-of-the-art research in the broad field of SiC classical and quantum photonics.

We will first describe SiC material optical properties relevant to its deployment in photonic devices, comprising of nonlinear optical properties.[25] We will then discuss optical emission by SiC defects such as donor−acceptor emitters,[26] used for light generation in white LEDs,[27] and point defects within the bandgap (color centers).[28]

We will then review the state of the art of SiC photonic components to be integrated in photonic circuits, specifically waveguides, 1D and 2D photonic crystal cavities, microdisk and microring resonators, based on doped thin layers[20] and thin layers of SiC on insulator (SiCOI).[29,30]

The role of SiC in emerging quantum technologies[7,31] will be the focus of the last section. We will describe the optically and electrically driven quantum emitters originating from color centers[13,32−34] and the current main challenges to achieve ideal single photon emission in this material, including their emission enhancement via material nanostructuring and their spectral and charge control in electrical devices.[35] Specifically, we will explain the role of SiC quantum emitters as spin-photon interfaces[24,36] for remote quantum entanglement,[37] quantum gates,[38] and quantum photonics.[20,39,40] We will also introduce novel applications and technologies in quantum sensing of the magnetic field,[41−47] electric field,[48−50] temperature,[51−53] and strain.[35,54−56] For quantum sensing applications, photonics can play a central role in enhancing the sensitivity and acquisition time of otherwise weak quantum processes and to improve integration and scalability of future devices.

In the conclusion, we critically analyze the challenges still remaining in this field, based on the results reported in the literature, and provide an outlook of future research that can lead to successful applications of SiC as a quantum and classical photonics platform.

A summary of the paper topics is presented in Figure 1.

https://doi.org/10.1021/acsphotonics.1c01775
ACS Photonics 2022, 9, 1434−1457

MATERIAL OPTICAL PROPERTIES

SiC is a polymporphic material, existing in a large variety of different crystal structures (polytypes). The hexagonal 4H-SiC (bandgap 3.23 eV) and 6H-SiC (bandgap 3.0 eV) polytypes are the most commonly available, together with the cubic 3C-SiC (bandgap 2.36 eV).

The hexagonal polytype, 4H-SiC, possesses a broad optical transparency (0.37−5.6 μm[57−59]), and it is birefringent, with ordinary and extraordinary refractive indexes measured in the visible and near-infrared. For standard wafers grown on the *c*-axis, the ordinary refractive index is in the plane of the wafer and corresponds to TE polarization, while the extraordinary refractive index is perpendicular to the plane of the wafer along the main *c*-crystallographic axis and aligns with TM polarization. Due to birefringence effects, phase-matching of the ordinary and extraordinary refractive indexes can be achieved with appropriate polarizations and propagation directions of the light traveling in SiC crystals. In Figure 2, the relevant optical

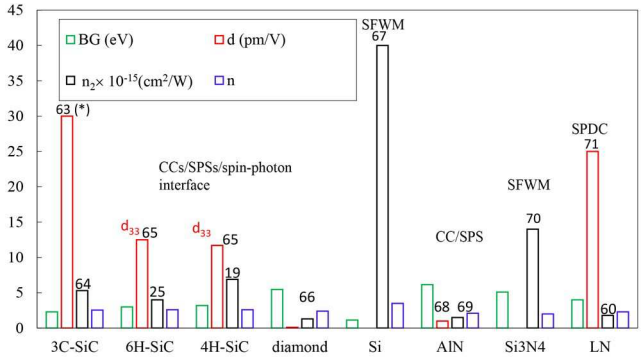

Figure 2. Visualization of the most typically quoted values of the bandgap (BG), linear refractive index (n), nonlinear refractive index (n_2), second order nonlinear coefficient (d) of the main SiC polytypes (3C-SiC, 6H-SiC, and 4H-SiC) at 1550 nm,[19,25,63−65] diamond,[66] Si,[67] AlN,[68,69] Si_3N_4,[70] LN.[60,71] (*) Represents a predicted value for 3C-SiC second-order nonlinearity. These are also the currently alternative photonic platform to the most commonly used Si and groups III−V materials (InP, GaAs,GaAs/AlGaAs). The mechanisms used for generation of the quantum state of light in the different materials are indicated as a result of their optical properties: spontaneous parametric down-conversion (SPDC), spontaneous four-wave mixing (SFWM), and color centers (CCs) responsible for single-photon sources (SPSs) and spin−photon interface. Among these platforms, only Si and LN are available as commercial wafer on-insulator SOI and LNOI, making them currently more accessible for QPIC.

properties of the main material photonic platforms (except groups III−V), such as linear refractive index (n), bandgap (BG), and nonlinear second (d), and third order coefficient (n2) are shown for comparison. While Si is the most used today due to the commercial availability of silicon on insulator (SOI) and the high n2 value, it does not possess second order nonlinearity and, due to its small bandgap, is affected by two-photon absorption at 1550 nm. The opposite occurs for lithium niobate, which has an excellent second order nonlinearity and is commercially available in thin films as lithium niobate on insulator, while its third-order nonlinearity is 3× lower[60] of SiC and comparable with Si_3N_4 and AlN.[61] While single photon emission based on color centers in lithium niobate has not been observed so far, the incorporation of rare-earth ions into lithium niobate integrated photonics can be achieved, possibly enabling optical quantum memories and qubits within PICs.[62]

While SiC has a relatively low refractive index compared to Si, it emerges as a material with a high second and third order nonlinearity, enabling frequency conversion and optical modulation, and a large bandgap providing the opportunity of bandgap active emitters such as donor−acceptor defects and color centers, which will be discussed in the following sections.

Nonlinear Optical Properties. SiC has been investigated for nonlinear optical properties in the visible[65] for many years and more recently also in the near-infrared.[64,72] These properties are relevant for PICs in order to achieve light confinement and propagation or storage, optical modulators, and emission frequency conversion. In the hexagonal polytypes 4H and 6H, SiC crystallizes in the point group *6mm*, while the 3C-crystal structure has a 43*m* symmetry, meaning they are noncentrosymmetric and birefringent uniaxial crystals with second-order nonlinear optical (NLO) effects.

Due to its birefringence, harmonic generation can be obtained with specific polarization using phase-matching of the ordinary and extraordinary refractive indexes. Second harmonic generation (SHG) has been demonstrated in all polytypes,[39,74,75] harnessing its quadratic nonlinearity $\chi_{ijk}^{(2)}$, with measured values reported ≈12.5 pm/V in the hexagonal polytypes[65] and estimated by first-principles simulation to be as high as 30 pm/V in the 3C polytype.[63] The third-order (Kerr[76,77]) nonlinearity $\chi_{ijk}^{(3)}$ (also known as nonlinear refractive index, n_2) is also important for its effects in optical propagation as waveguiding,[58,78] with a value of 8.6×10^{-19} m^2/W at 2360 nm[78] and of 6.9×10^{-19} m^2/W at 1550 nm[19] for 4H-SiC. For 3C-SiC, it has been estimated to be 4.87×10^{-19} m^2/W at 1567 nm[77] and measured 5.31×10^{-19} m^2/W at 1550 nm.[64] More recently, the nonlinear refractive index coefficient of the order of 10^{-18}−10^{-19} m^2/W[59] and nonlinear absorption coefficients (2 photon of the order of ≈10^{-13}−10^{-11} m/W and 3 photon-absorption coefficient of the order of 10^{-28}−10^{-27} m^3/W^2) for semi-insulating 6H-SiC and 4H-SiC were measured from 400 to 1000 nm.[25] Values of n_2 above 1000 nm for all three polytypes are estimated in.[77] The wavelength dependence of the multiphoton absorption is relevant for better femtosecond laser fabrication and design of ultrafast all-optical switching in SiC.

By nanostructuring SiC and improving the quality factor (*Q*) of the microring and microdisk resonators, NLO effects based on second-order and third-order nonlinear coefficients have been recently enhanced and observed (Figure 3a). Generally, the NLO response of 3C, 4H, and 6H-SiC nanostructures covering the optical spectrum from the visible through the mid-infrared and far-infrared, could open up a wide range of applications such as wavelength conversion, four-wave mixing (FWM) observed in both 4H and 3C-SiC,[64,79,80] second/third/fourth-harmonic generation observed in 4H-SiC microdisk resonators[73] (Figure 3b−e), SHG, and difference frequency generation (DFG) in 3C-SiCOI microring resonators and waveguides,[81] optical parametric oscillator (OPO) in 4H-SiC microring resonators,[19,82] parametric amplification in 4H-SiC crystal,[83] frequency comb generation[19,84] (achieved with the lowest possible power generation efficiency after AlGaAs on-insulator[85]; Figure 3f), self-phase modulation, and supercontinuum generation in 6H-SiC crystal[86] from 1.3 to 2.4 μm. Nonlinear optical properties in 4H-SiC have been also investigated in the mid-infrared (mid-IR) where broadband emission from 3.90 to 5.60 μm[57] was obtained from DFG. Phase-matched DFG was found to be possible in 4H-SiC up to the far-IR (THz) region beyond 17 μm.[87] In the far-IR region SiC also exhibits surface phonon-polariton (SPhP) sharp

https://doi.org/10.1021/acsphotonics.1c01775
ACS Photonics 2022, 9, 1434−1457

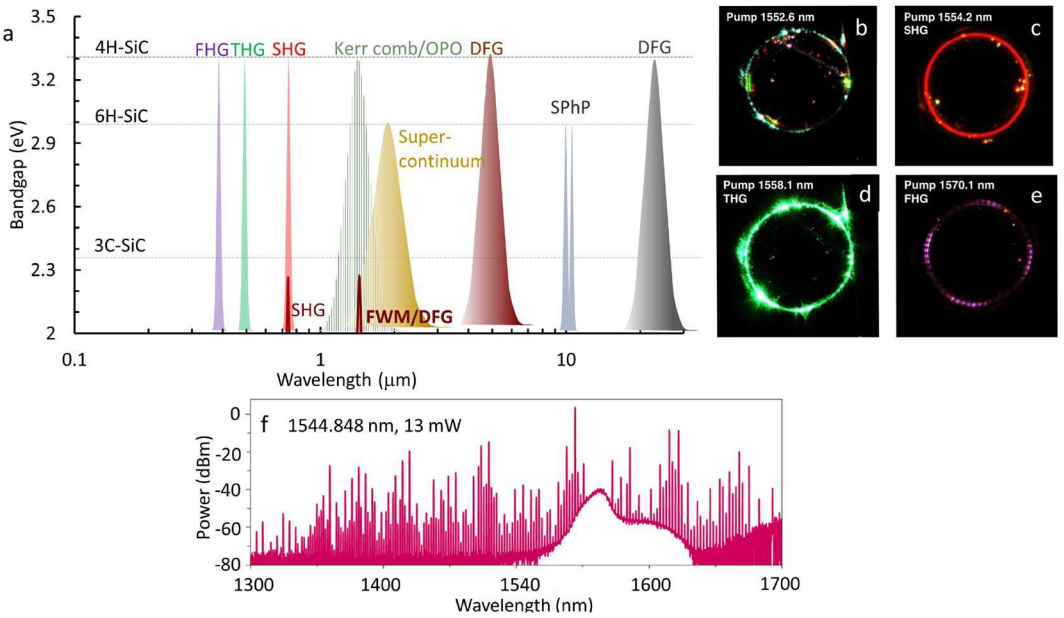

Figure 3. (a) Illustration of the spectral coverage, from the visible to the far-infrared, of the nonlinear emission generation observed in 3C-, 6H-, and 4H-SiC. (b–e) Nonlinear frequency generation in microdisk resonators: second harmonic generation (SHG), third harmonic generation (THG), and fourth harmonic generation (FHG) at 776.3, 517.5, and 388 nm, respectively. (f) Broadband Kerr frequency comb generations from 1300 to 1700 nm, with a 13 mW pump at 1544.848 nm in high $Q \approx 6.75 \times 10^6$ 4H-SiCOI microresonators. Images in (b) are reprinted in part with permission from ref 73. Copyright 2021 Springer Nature under the https://creativecommons.org/licenses/by/4.0/.

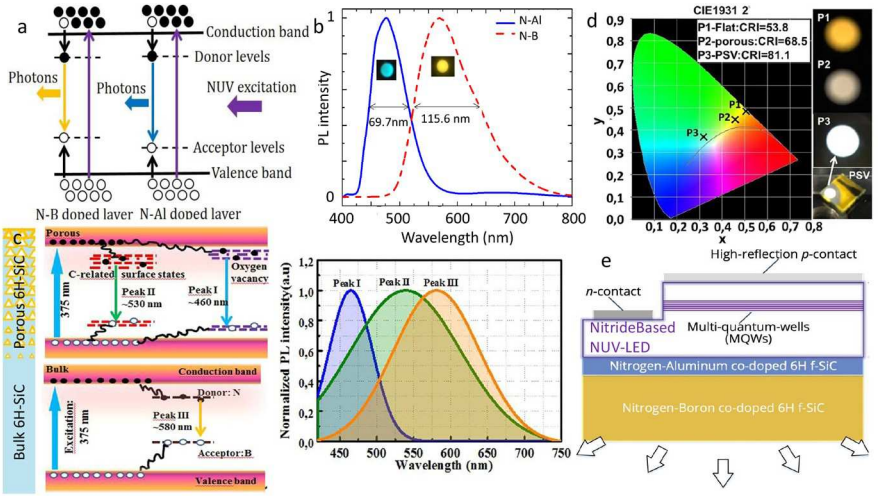

Figure 4. Overview of novel schemes for SiC LED. (a) Schematic drawing of donor–acceptor pair recombination mechanism in 6H-SiC. After NUV pump, the N–B pair will emit yellow light and N–Al will emit blue light. (b) Photoluminescence spectra of N–Al and N–B pairs under the excitation of 375 nm laser. Their corresponding camera images are inserted under the spectral peak. Blue N–Al spectrum has a full width at half-maximum (fwhm) of 69.7 nm and yellow N–B spectrum has fwhm of 115.6 nm. The large fwhm is beneficial to achieve high CRI for white light sources. (c) Schematic diagram of the fluorescent 6H-SiC with porous surface layer. Three possible transitions in fluorescent 6H-SiC are shown: DAP recombination (peak III) in the bulk layer, the transition through C-related (peak II) and oxygen vacancy-related (peak I) surface defects in the porous layer. Schematic of the normalized emission spectra from porous layer (peaks I and II) and fluorescent bulk layer (peak III). (d) Chromaticity diagram showing the color of the light emitted from fluorescent flat (P1), porous sample before passivation (P2), and porous sample after passivation (P3), the corresponding CRI is 53.8, 68.5, and 81.1, respectively. The inset figures are camera photos of observed luminescence in the corresponding flat, porous sample before and after passivation. (e) Schematic diagram of the stacking structure of a white LED based on N–B and N–Al codoped f-SiC thin films. (c, d) Reprinted in part with permission from ref 27. Copyright 2017 Springer Nature under https://creativecommons.org/licenses/by/4.0/. (e) Reprinted in part with permission from ref 95. Copyright 2019 American Chemical Society.

resonances at ≈10.9 μm (generally observed between 10 and 12 μm[88–90]). This emission has also been investigated by infrared-visible sum-frequency generation microscopy in 6H-SiC nanophotonic structures.[91] The dielectric function for 4H-SiC exhibits a near-zero point at 10.3 μm, close to the LO phonon frequency, and a pole (point of extremely high permittivity) at 12.55 μm, close to the TO phonon frequency. Because of this, by combining SiC as substrate with plasmonic antennas the radiation pattern is strongly modified in the mid-infrared region close to the LO and TO. For plasmonic antennas with resonance

https://doi.org/10.1021/acsphotonics.1c01775
ACS Photonics 2022, 9, 1434–1457

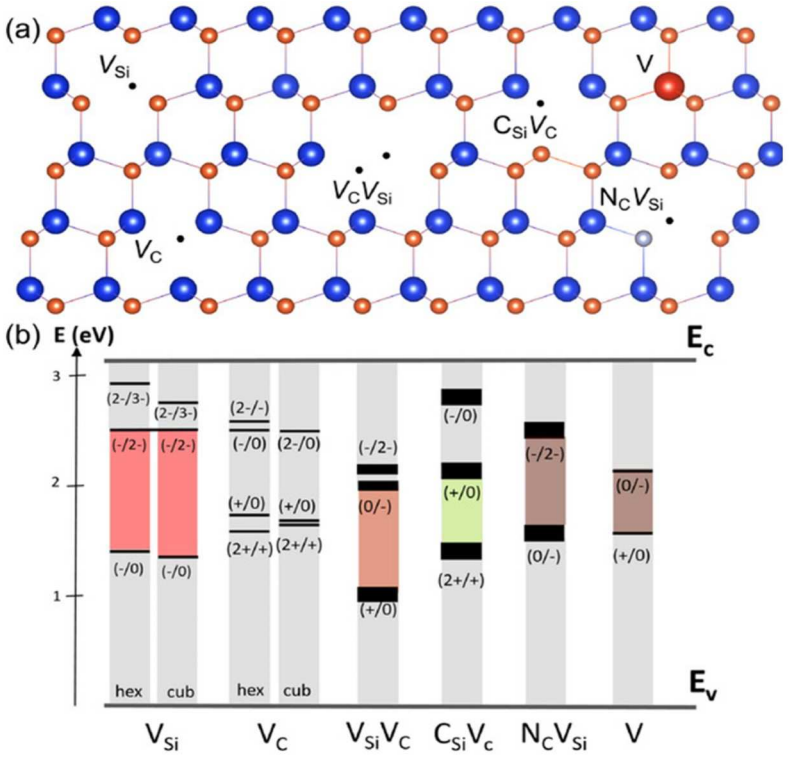

Figure 5. (a) Overview of the main color centers studied in SiC V_C, V_{Si}, the divacancy $V_{Si}V_C$, the carbon antisite vacancy pair $C_{Si}V_C$, Vanadium (V) impurities, and N_CV_{Si} as they appear in the hexagonal lattice of the 4H-SiC. (b) Their energy levels and charge states, with the quantum compatible charge states in color code. Figure reprinted with permission from ref 32. Copyright 2021 Wiley-VCH under https://creativecommons.org/licenses/by/4.0/.

approaching these two points, the SiC substrate controls the radiation pattern.[92] This effect can be used for controlling the plasmon resonance of metamaterials.

Donor−Acceptor Pairs. SiC is an appealing material to develop light sources. Its small lattice is mismatched to gallium nitride (GaN), which has enabled it as an excellent substrate for GaN-based, light-emitting diodes (LEDs). Additionally, it has exceptional optoelectronic properties[72,93] of its own, good thermal conductivity,[94] is abundant and stable in harsh environments.

Despite its indirect bandgap, SiC has been known as an optically active material with photoluminescence (PL) in the bulk.[95] Light emission does not originate from the band−band recombination, but from defects due to the presence of donor−acceptor pairs,[96] surface defects, and point defects within the bandgap.[97] Remarkably, the first blue light-emitting diode (LED), reported in 1907, was made of SiC,[98] and greenish SiC LED was demonstrated in ref 99. This is quite important for white-light generation, as this is normally accomplished by additively mixing three primary colors of red, green, and blue, or at least two of them with a relatively lower color rendering index (CRI). Therefore, the development of white LEDs based on these primary colors emission from SiC has had more than one century history.[100]

By combining nanostructuring[101] with various donor−acceptor emission (such as nitrogen−boron and nitrogen−aluminum), white light-emitting diodes (LED) have been produced.[27] Recently, doping SiC heavily with donor−acceptor pairs, such as nitrogen−boron pairs and nitrogen−aluminum pairs, has been investigated to fabricate novel white light sources, where SiC is working as a wavelength converter and substrate for the near-ultraviolet LED as a pump.[95,96] This fluorescent SiC (f-SiC) based white LED is expected to have high efficiency, high CRI, and a long lifespan, even in a harsh environment. The emission mechanism of N−Al and N−B pairs is shown in Figure 4a,b. The energy levels of Al, B, and N in the bandgap of 6H-SiC produce the blue emission from the N−Al pair and a yellow emission from the N−B pair. Thus, the mixture of them could provide high CRI (Figure 4d) white light because of the wide full width at half-maximum (fwhm), that is, 69.7 nm for N−Al and 115.6 nm for N−B. For the state of the art, the quantum yield of the yellow N−B emission is about 30%, and the main limiting factor is the Auger recombination because of the high concentration doping of N and B.[95] The blue N−Al emission is still much lower in efficiency compared to N−B emission.

Due to the rather low efficiency of blue emission from N−Al pair, porous SiC is studied as an alternative for blue emission to achieve high color index white light sources. Porous SiC is fabricated by anode oxidation, the same method used for porous Si fabrication. After optimization of anode oxidation parameters and passivation parameters, strong blue emission is realized from porous SiC.[27] The emission of porous SiC is ascribed to surface related defects. As shown in Figure 4c, there are two types of defects, for example, C related surface states and oxygen vacancies, which contribute to the green and blue peak, respectively. When blue-emitting porous SiC is fabricated on the surface of a yellow-emitting SiC Figure 4e, white light with CRI as high as 81.1 is demonstrated, and shown in Figure 4d.

Color Centers. Recent advances in material purity control have enabled the reassessment of intrinsic SiC point defects[28,97] with a better assignment and understanding of their spin and charge state properties. These defects or color centers include

https://doi.org/10.1021/acsphotonics.1c01775
ACS Photonics 2022, 9, 1434−1457

the negatively charged silicon vacancy (V_{Si}^-) centers;[102−104] the divacancy,[105−109] consisting of neighboring C and Si vacancies; the carbon antisite vacancy pair ($C_{Si}V_C$), a carbon atom replacing a silicon vacancy close to a carbon vacancy.[23,110−114] Other extrinsic defects are the nitrogen vacancy (N_CV_{Si}) centers;[115−119] transition metal impurities,[120] such as chromium,[121] molybdenum,[122,123] and vanadium.[124,125] In addition, other unknown origin emitters have been recently found in SiC with emission in the near-infrared.[126]

Most of the above defects have a spin state and can act as solid state quantum bits and SPSs.[6,7,13,31,106,127,128] One of the mechanism to read out the spin state is via optically detected magnetic resonance (ODMR), consisting in a spin-dependent fluorescence in the presence of magnetic field and/or microwave excitation. After initial optical excitation, the defect, generally a triplet, is polarized in the ground spin state via spontaneous emission of the spin conserving transitions between the excited state and the ground state and the spin nonconserving transitions to a nonradiative long life metastable state. An overview of the main defects is shown in Figure 5 and a full description of each of them is provided in ref 128 and references therein.

Silicon Vacancy. Negatively charged silicon vacancy (V_{Si}^-) centers are one of the most studied defects in SiC.[10,11,24,36,38,39,42,45,51,53,102−104,129−153] They are formed by a missing silicon atom in the SiC lattice that captures an additional electron. Spin-optical properties of V_{Si}^- centers vary slightly depending on the SiC polytype that is used and the (nonequivalent) lattice site from which the silicon atom is removed. Most studied are the two (three) distinct V_{Si}^- centers in 4H-SiC (6H-SiC) .[130,132] The optical properties of V_{Si}^- centers are most studied in the 4H polytype, exhibiting a zero phonon line (ZPL) emission at 862 nm for the V1 for the hexagonal lattice site center, and 917 nm for the cubic lattice site center, V2. In the 6H-SiC polytype, the V1, V2, and V3 centers show ZPLs at 865, 887, and 906 nm, respectively.[154,155] Additionally, V_{Si}^- centers have been observed in the 15R polytype.[136,151,156] The spin quantum number of all V_{Si}^- centers is $S = 3/2$.

Spin coherence times of 1.4 ms (20 ms) have been measured for single defects[38] in isotopically modified SiC (dynamically decoupled ensembles and natural SiC[10]). The magnetic dipole orientations of all V_{Si}^- centers is along the crystal *c*-axis, which is convenient for maximizing signal strength in quantum sensing based on well-orchestrated V_{Si}^- center ensembles. In this regard, most quantum sensing demonstrations have been performed using the so-called V2 V_{Si}^- center in 4H-SiC at 917 nm, as it shows an ODMR signal even at room temperature (see ref 128 and references therein). Recently, similar signal strengths have been obtained with V1 and V3 V_{Si}^- centers in 6H-SiC.[152] Sensing and high-fidelity control of nuclear spins surrounding individual V_{Si}^- centers was also demonstrated, which is an important ingredient toward quantum computing and quantum memory applications.[24,38] To boost detected optical signal strengths for those near-infrared emitters, most studies employ optimized optical structures, such as solid immersion lenses or nanopillars.

Divacancy. Divacancies (VV)[105−109] found in all polytypes, in 4H-SiC exist in four configurations, depending on the involved lattice sites, each identifiable by a different wavelength for the ZPL (*c*-axis oriented: (*kk*) 1131 nm, (*hh*) 1132 nm, basal: 1108 nm, 1078 nm). Their emission in the 1100 nm range, while not directly in the telecom band, is still advantageous in terms of fiber transmission, compared to the NV center in diamond (0.7 dB/km at ∼1100 nm vs ∼8 dB/km at 637 nm). Because of their C_{3v} symmetry with six active electrons, the VV in 3C-SiC and the (*hh*) and (*kk*) sites of divacancy in 4H-SiC feature a ^{3}E excited state, similar to the NV center in diamond, with six spin-selective transitions (E_x, E_y, A_1, A_2, E_1, E_2). In the limit of low-strain, E_x and E_y are "cycling" transitions, that maintain a purely $m_s = 0$ character and can be used for spin-readout with minimal decay probability into $m_s = \pm 1$.[157] PL excitation experiments[157] on individual VV have demonstrated narrow spin-selected optical transitions in both 3C and 4H-SiC, with line widths of the order of ∼100 MHz for 4H-SiC (that can be reduced to ∼20 MHz by electrical control[49]) and ∼1−2 GHz for 3C-SiC (probably related to much higher nitrogen concentration in the sample). Remarkably, orbital mixing for the (*hh*) and (*kk*) VV in 4H-SiC is about 1 order of magnitude smaller than for the NV center in diamond,[157] which is expected to lead to smaller optically induced spin-flips, potentially facilitating single-shot spin readout and spin-photon interfacing experiments using a photonic cavity.

The orbital and spin energy levels for the basally oriented (*kh*) divacancy are quite different than what discussed above, featuring a C_{1h} symmetry with a spin-1 orbital singlet ground state and orbital doublet excited state in the SiC electronic bandgap. The quantization axis is tilted at an angle of 71° with respect to the crystal *c* axis.[48] The C_{1h} symmetry imparts longitudinal (D_{GS}) and transverse (E_{GS}) zero-field splittings, so that the eigenstates are a superposition of S_z basis states.[48] In the excited state, the C_{1h} symmetry results in a transverse crystal field, which produces two widely separated 3A′ and 3A″ orbitals (with only 3A′ producing detectable luminescence). Each orbital has three spin sublevels, also featuring spin mixing due the presence of longitudinal (D_{ES}) and transverse (E_{ES}) zero-field splittings. Spin-selective optical transitions between the ground and excited state have been observed.[48] Remarkably, the basally oriented (*kh*) VV in 4H SiC has been shown to possess a clock transition, with reduced sensitivity to magnetic noise, close to zero magnetic field.[158] This noise-protected qubit is achieved by applying microwave dressing to its ground-state electron spin. This has been exploited to demonstrate a record inhomogeneous dephasing time T_2^* of ∼22 ms for the electronic spin in SiC with natural abundance of nuclear spins and an associated T_2 coherence time of 64 ms. Using avoided crossings between the electronic levels of VV, a suppression of fluctuating charge impurities and an increased coherence time at clock transition were observed.[159] This result indicates the opportunity to design single spin devices operating in these points.

Carbon Antisite Vacancy Pair. The $C_{Si}V_C$ can be found in all SiC polytypes and it can be converted from the V_{Si} by annealing at 700−750°.[150] The positively charged state $C_{Si}V_C^{(+)}$ was initially identified[110] in 4H-SiC. Its PL in ensemble is associated with eight ZPLs due to four inequivalent sites with two excited states and are also known as AB-lines (A1 = 648.7 nm, A2 = 651.8 nm, A3 = 665.1 nm, A4 = 668.5 nm, B = 671.7 nm, B2 = 673 nm, B3 = 675.2 nm, B4 = 676.5 nm).[23] This center has a C_{3v} (C_{1h}) symmetry for the axial (basal) configuration, and due to the spin number $S = 1/2$, no ODMR has been observed yet. Its neutral charge state is predicted to have an emission in the infrared and $S = 1$ based on ab initio simulations,[112] however, it is not accessible in n-type and p-type materials and it has been studied recently in ultrapure isotope-enriched 4H−^{28}SiC.[113] Using photons with a wavelength shorter than 539 nm, the center can change its charge state from positive to neutral; as

https://doi.org/10.1021/acsphotonics.1c01775
ACS Photonics 2022, 9, 1434−1457

such, by careful design of the material purity, the $C_{Si}V_C^{(0)}$ can be controlled by optical excitation and converted from $C_{Si}V_C^{(+)}$.

Other Centers. While V_{Si} centers and VV have been the most studied centers in SiC for quantum technology, other centers are currently attracting interest. Nitrogen vacancy (NV) or N_CV_{Si} centers exist also in all SiC polytypes,[115−119,160] with four configurations featuring ZPLs closer to the telecom range, between 1175 and 1250 nm. Coherent spin control has been demonstrated for both ensembles and single NV centers, up to room temperature.[119] Given that, in the negatively charged state, it has the same electronic structure as NV centers in diamond (with a $^3A_2$ ground state and a ^3E excited state), one can expect similar spin-photon interfacing protocols to be valid.

Recent work has demonstrated control of electronic spins associated with transition metal impurities,[120] such as chromium,[121] molybdenum,[122,123] and vanadium.[124,125] Vanadium (V^{4+}) is particularly appealing since it features ZPLs directly in the telecom O-band, with excited state lifetimes on the order of tens of nanoseconds, and a $S = 1/2$ electronic spin, corresponding to a single unpaired electron coupled to the ^{51}V nuclear spin ($I = 7/2$). Single vanadium centers have been isolated, and ODMR has been demonstrated.[124] The T_1 spin relaxation time appears to be in the μs time scale at $T = 3.3$ K, but is expected to improve at lower temperatures. Interestingly, the optical transitions are affected by mass shifts of nearby silicon and carbon isotopes, which may provide a pathway toward optically resolved nuclear spins.[124] Longer spin relaxation time scales have been demonstrated in experiments with ensemble molybdenum impurities,[123] reaching seconds at a temperature of ∼2 K.

A general theoretical framework to develop spin control and spin-photon interfacing in these systems has been put forward,[120] using group-theoretical considerations in the case of a spin 1/2 single electron in a *d*-shell for C_{3v} symmetry, together with an analysis of nuclear-electron hyperfine couplings, useful to implement quantum memory schemes.[161]

PHOTONIC TECHNOLOGIES

Background of Fabrication Approaches. A crucial prerequisite to the demonstration of integrated photonic devices is the availability of thin (wavelength-scale) membranes with well-controlled thickness, high material purity, and minimal surface roughness.

Different techniques have been proposed for the fabrication of high-quality SiC membranes, including the smart-cut process in 4H-SiC to achieve SiCOI,[162] 3C-SiC heteroepitaxially grown on a Si substrate thinned down where the silicon is then undercut,[163] photoelectrochemical etching of doped epilayers of 4H-SiC,[164] wafer bonding and thin down for both 3C and 4H-SiC,[30,165] two-step reactive ion etching, and angle etching in 4H-SiC.[38]

4H-SiC epitaxial layers can only be grown on SiC substrates, so that selective etching techniques, routinely used for example in the III−V platform, are not available. One powerful approach for photonics fabrication in SiC is based on the SiC-on-insulator (SiCOI) technology that promises large-scale production capabilities due to its industrial relevance and CMOS compatibility.[19,39,75] The first SiCOI structures were demonstrated in 1997 using the smart-cut process,[166] and SiCOI nanophotonic structures were subsequently fabricated.[74,78,167] Recently wafer-scale 4H-SiCOI was optimized by ion-cutting and layer transferring[29] and microring resonators with quality factors of 6.6×10^4 were achieved, providing a integrated nonlinear photonic platform.[82]

Ion irradiation in the smart-cut process, however, induces lattice damage which increases optical absorption within the structure,[59] limiting the *Q*-factor below 10^5, and is detrimental for the quantum coherence properties of the targeted spin centers.

Less-damaging thin-film epitaxy techniques using wafer bonding have been applied in both 3C-SiC[30,81,168] (leading to microresonators in 3C-SiC with *Q* above 10^5) and 4H-SiC[19,39,75,165] to achieve SiCOI. In 4H-SiC this technique maintains the pristine "quantum-grade" quality of bulk epitaxially grown 4H-SiC. In 4H-SiC thermally oxidized SiC is fusion-bond to a SiO_2-on-Si handle wafer, and the SiC layer is subsequently thinned down to a few 100 nm thickness using industry-compatible grinding and chemical-mechanical polishing steps. In the end, nanophotonic structures are created using electron-beam lithography and SF_6/O_2 plasma etching. With this method, wafer-scale 4H-SiCOI have been obtained.[73]

Another approach to create suspended membranes in addition to removing part of the Si substrate, is based on photoelectrochemical etching of doped epilayers of 4H-SiC.[169,170] This approach may induce material degradation and porosification. A further approach is based on a two-step reactive ion etching and angle etching in 4H-SiC.[38]

3C-SiC can be grown on a Si substrate, in principle allowing the possibility to create membranes by material-selective etching. Suspended membranes obtained from 3C-SiC on Si, however, suffer from the low quality of the SiC/Si interface, with losses of 21 dB/cm at 1550 nm wavelength.[163]

Waveguides. Waveguides are core components of PICs and have a relevant role in QPICs, to transfer quantum information from a quantum node to another[165] or to store information in a cavity, such as a ring resonator, where nonlinear properties are enhanced and frequency conversion can occur. They can confine light and propagate light simply by total internal reflection in a high refractive index material. The first attempt to fabricate waveguides in SiC dates back to 1991,[171] where light confinement was achieved in a thin 3C-SiC layer transferred onto a sapphire substrate. 4H-SiCOI based on smart cut,[78] and 3C-SiC heteroepitaxially grown on a Si substrate with silicon undercut[163] were initially used for waveguides fabrication and testing, suffering of high losses. Recently suspended waveguides were obtained in 3C-SiC combined with post fabrication thermal annealing in high temperature oxygen atmosphere and a new etching process. Here the annealing reduced significantly the surface roughness and the crystal defect density such as stacking faults and antiphase boundaries at the SiC-Si interface, overall reducing the waveguide loss to 7 dB/cm.[172]

High nonlinearity and low loss were found also in waveguides and ring resonators fabricated in amorphous SiC (a-SiC) grown directly on silica, using plasma-enhanced chemical vapor deposition, with loss as low as 3 dB/cm,[72] providing a very scalable material growth.

High quality SiCOI obtained by wafer bonding and thin down for both 3C and 4H-SiC[30,165] has achieved waveguides losses as low <0.4 dB/cm.[19]

Using angle etching techniques to fabricate triangular waveguides, color centers were integrated within the waveguide with similar optical and spin-properties of the pristine material, permitting quantum gates operation using nuclear spins coupled with single V_{Si} spin defects.[38] The triangular waveguides

https://doi.org/10.1021/acsphotonics.1c01775
ACS Photonics 2022, 9, 1434−1457

geometry has been studied for the future aim to fabricate high cooperativity photonic cavities.[17]

1D-2D Photonic Crystal Cavities. Photonic crystals cavities were among the first photonic devices to be explored in silicon carbide due to their ability to confine light in subwavelength volumes, thus enhancing the light and matter interaction. The exploration started in smart-cut layers of 6H-SiC,[167,173,174] heteroepitaxially grown 3C-SiC on silicon,[175,176] and amorphous SiC layers deposited on silicon.[177] These platforms were used for implementation of the 2D heterostructure and L3 photonic crystal cavities with quality factors up to $Q \sim 10000$, and the 1D nanobeam cavities with $Q \sim 70000$, suitable for nonlinear optics (SHG[74]) and optomechanics. Here, the nanoscale mode volumes of $V \sim \frac{1}{2}\left(\frac{\lambda}{n}\right)^3$ achieves the light−matter interaction at levels unreachable in macroscopic devices. However, as the field started focusing on color center photonics, these substrates proved unfit for hosting optically stable emitters with narrow line widths. In particular color center emission enhancement was first achieved in 3C-SiC photonic crystal and the optical and spin properties of the color center integrated in nanophotonics were found to be deteriorated compared to the pristine material.[178] Remarkable results have been achieved with 1D photonic crystal cavities fabricated via doping selective photoelectrochemical etching in 4H-SiC, enabling the first demonstration of Purcell enhancement of emission from V_{Si} ensembles.[179] Using the same photonic crystal fabrication method, coherent spin control of a single VV integrated into photonic crystal cavities was realized with a coherence time of 7.3 μs, which is however lower than in pristine material (1 ms).[180] Using improved SiCOI platform,[39,75] and angled etching,[169] photonic crystal with quality factors in the range 5000−630000 were fabricated, and they were further explored for quantum photonics, isolating single V_{Si},[39] nonlinear optics,[75] and coherent spin manipulations.[180]

Microring Resonators. Microring resonators, together with waveguides, are essential components in PICs for field enhancement, spectral filtering and thus frequency conversion efficiency enhancement. Kerr nonlinearity was enhanced by suspended microring resonators achieving FWM in 3C-SiC on Si substrate.[64] Quality factors were in the range 11000−24000. Recently, a quality factor of 3C-SiC suspended microring resonators of over 41000 were achieved with postfabrication thermal annealing to minimize optical propagation losses.[172] FWM was also achieved in $Q \approx 70000$ microring resonators obtained in amorphous a-SiC on silica.[181] Using a low-temperature hydrophilic bonding process followed by chemical-mechanical polishing, 3C-SiCOI were prepared obtaining $Q \approx 30000$. Only recently, electro-optical modulation was achieved in microring resonators and waveguides with integrated electro-optical phase-shifters.[182,183] The first prototypes of angle-etched microring resonators have been recently demonstrated using Faraday-cage etching method[184] measuring resonances with quality factors of 3500.

Using 4H-SiCOI obtained from smart cut wafer the highest Q of microring resonators obtained is 7.3×10^4,[59] while using wafer bonding and thinning down technique microring resonators were fabricated with $Q \approx 7.8 \times 10^5$,[39] $Q \approx 1.1 \times 10^6$ to achieve for the first OPO in SiC,[19] and $Q \approx 5.6 \times 10^6$ to study the quantum effects in soliton microcombs.[84] Dual-pump OPO has been demonstrated also in smart-cut 4H-SiCOI ring resonators;[82] thermal effects on optical power absorption and thermal tuning broadband solitons were studied. Third-order nonlinearity in 4H-SiC is polarization-dependent and all the above FMW processes were demonstrated with TE polarized light or ordinary polarization. Recently extraordinary polarization (TM polarized light) FWM has been demonstrated to be more efficient than the ordinary polarization.[79]

Microdisk Resonators. Microdisk resonators support whispering gallery modes with volumes of several or more cubic wavelengths. Among their advantages is the multitude of TE and TM polarized resonances which can be used to couple to emitters of various orientations at visible and NIR wavelengths. Initially fabricated in 3C-SiC based on thin-film epitaxy techniques on silicon undercutting the underlying silicon substrate,[30,168,185,186] with a maximum Q factor around $Q \sim 25000$. Microdisks in 4H-SiC were first fabricated through photoelectrochemical etching in p-doped SiC[187] with quality factors approaching $Q \sim 10000$ at 2 μm diameters which enhanced the emission of the intrinsic material PL in the 600−900 nm range. Similar devices were subsequently implemented in 3C-SiC on silicon using plasma and gas phase etching,[188] where experimental differentiation between TE and TM polarized modes was achieved. In further efforts to integrate emitters with microdisks in 3C-SiC, surface oxidation induced single photon emitters were precharacterized and aligned with the device pattern resulting in up to 1900 quality factor whispering gallery modes.[189] Increasing the diameter of the device above 10 μm reduced losses to $Q \sim 50000$,[39] however, the increased mode volume rendered these devices less appealing for emitter integration due to the overall reduction in light−matter interaction strength. Integration with an external nanodiamond has also been explored to enhance diamond color center emission in a hybrid device.[190] Microdisk resonators were fabricated in 4H-SiCOI using smart cut and achieving quality factor around 5000.[191] Microdisk resonators with over 7 million optical Q based on 4H-SiCOI wafer-bonding and thinning techniques, as described below, have been used to enhance second and third order harmonic generation and frequency combs and they are among the most promising nonlinear optical devices in this material.[73] The applications of SiC microdisk resonators include probing of the breast cancer cells[192] and torsional resonators.[193] Microdisk resonators in SiC have also application in opto-mechanics[194−196] due to SiC excellent mechanical properties reaching high mechanical $Q \approx 10^5$ and high (3−30 MHz) frequency. This permits sufficient strong opto-mechanical mode coupling to observe thermal Brownian motions of mechanical modes at room temperature.[197]

Silicon Carbide on Insulator (SiCOI): Toward Integrated Chips. A strong research effort is currently devoted to the creation of integrated photonics chip comprising different elements on a SiCOI platform.

Using the wafer bonding and thinning down technique described above, Lukin et al. integrated single quantum emitters (silicon vacancy centers) into suspended nanophotonic SiC resonators.[39] Thanks to the low waveguide loss (<0.5 dB/cm), record cavity photonic crystal quality factors of up to $Q \sim 1.5 \times 10^4$ were achieved, leading to a 120-fold improvement of the fluorescence rate of a single emitter.

The unparalleled and unique versatility of the SiCOI approach is further highlighted using SiC microring resonators in nonlinear optics experiments. Initial experiments showed second harmonic generation efficiencies of up to 360%/W, suggesting that on-chip quantum frequency conversion from the emission wavelength of silicon vacancy centers to the telecom range could be achieved with pump powers below 1 mW.

https://doi.org/10.1021/acsphotonics.1c01775
ACS Photonics 2022, 9, 1434−1457

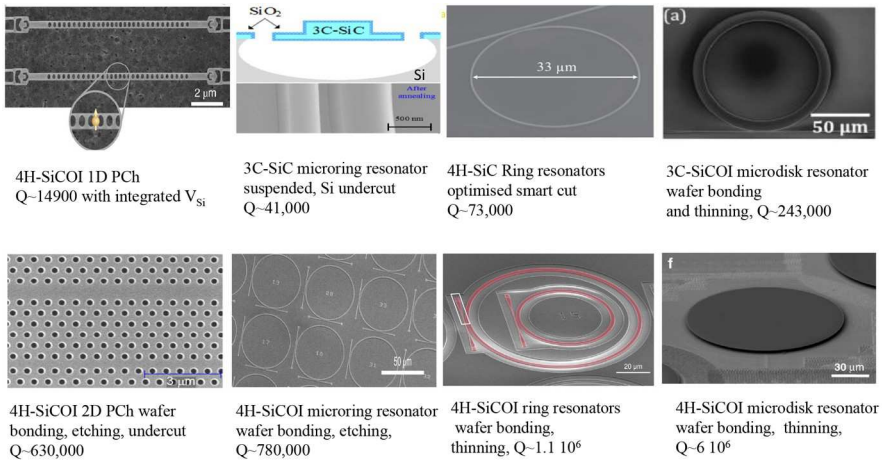

Figure 6. Summary of the most recent photonic cavities in SiC, from top left to the right and below: 4H-SiCOI 1D suspended nanobeam array photonic crystal, reprinted with permission from ref 39. Copyright 2020 Springer Nature; suspended microring resonator obtained undercutting silicon from 3C-SiC thin film hepitaxially grown and optimized with high temperature annealing in oxygen, adapted with permission from ref 172. Copyright 2020 The Optical Society; microring resonator fabricated with an optimized smart cut technique in 4H-SiC, reprinted with permission from ref 59. Copyright 2019 The Optical Society; 3C-SiCOI microdisk resonator reprinted with permission from ref 168. Copyright 2019 The Optical Society; 4H-SiCOI photonic crystal cavity reprinted in part with permission from ref 75. Copyright 2019 The Optical Society; 4H-SiCOI microring resonators obtained by wafer bonding, undercutting and thinning reproduced with permission from ref 39. Copyright 2020 Springer Nature; 4H-SiCOI ring resonator reproduced with permission from ref 19. Copyright 2020 The Optical Society; 4H-SiC microdisk resonator, reprinted with permission from ref 73. Copyright 2021 Springer Nature under https://creativecommons.org/licenses/by/4.0/.

Subsequent improvements in nanofabrication reduced waveguide loss to 0.38 dB/cm, resulting in quality factors exceeding one million, which enabled efficient FWM and generation of telecom-wavelength−frequency combs with pump threshold levels comparable to silicon nitride devices.[19] Those results showed further that the intrinsic optical absorption of 4H-SiC is well below 0.1 dB/cm. In more recent work, the fabrication of a ring resonator a $Q = 5.6 \times 10^6$ has been reported, with losses 0.08 dB/cm.[84] A record $Q = 6.75 \times 10^6$ was recently demonstrated on a 4H-SiCOI platform microdisk resonators, enabling multiple order frequency generation, cascaded Raman lasing, broadband Kerr frequency combs from 1300 to 1700 nm.[73] It will be interesting to explore whether those loss levels can be reached toward achieving ring resonators with quality factors exceeding 10^7.

To use SiCOI devices for quantum communication, where optical losses need to be minimized, as amplification is not possible, one crucial challenge is to improve coupling efficiencies from on-chip waveguides to optical fibers, potentially using adiabatic transitions in tapered waveguides.[198,199]

A summary of various photonic cavities recently fabricated in SiC and SiCOI as comparison with progressively higher quality factor (in the near telecom or telecom wavelength) is provided in Figure 6.

QUANTUM PHOTONIC TECHNOLOGIES

Single Photon Emitters. Most of the color centers described above have been optically addressed at the single defect level showing single photon emission.[6,13,128] The brightest SPSs in SiC have been observed in the visible range (649−677 nm) assigned to $C_{Si}V_C^{(+)}$ in 4H-SiC, cubic 3C-SiC nanoparticles,[200] and 3C-4H SiC nanotetrapods.[201] Fully polarized SPSs in a broader visible region (545 to 750 nm) were formed also by annealing,[202] oxidation at 800° in SiC polytypes substrates,[203] by wet-oxidation 4H-SiC MOSFETs,[204] their physical origin appears at the SiC/SiO_2 interface,[205] while they have unknown structure assignment; also a 3C polytype inclusion during epitaxial 4H-SiC growth has not been excluded. Their unknown origin limits their on-demand localized engineering and their spectral diffusion is a limitation for application in quantum technologies. Due to the variety of SiC emitters in this spectral region, their spectral purity and integration within photonic cavities has not yet been fully investigated. The V_{Si} has been studied as a SPS in 4H-SiC[45,134] for all its optical transitions associated with the cubic and hexagonal sites, known as V1, V1′, and V2, depending on their location in the lattice and degeneracy of the excited state. For this defect, the verification of the single photon indistinguishability has been demonstrated, regardless of the lack of the center inversion symmetry, using solid immersion lenses.[36] The use of this defect for spin-photon interface will be discussed in the next section. The spectral broadening of this emitter has been measured to be 24 and 40 MHz, which is close to its Fourier-transform limited lifetime of 22.5 MHz.[38] To further narrowing its line width, a combination of charge depletion in ultrapure material and annealing can also be used, also improving spin measurements fidelity. The neutral VV was also characterized as a SPS in 4H-SiC at 20 K,[107] however, due to the low count rate, photon collection enhancement, and control is here essential. The ZPL line width of these emitters is close to their lifetime limit, which is ≈11 MHz, with a measured spectral broadening from 80 MHz[157] to a lowest of 20 MHz.[48] A SPS in the near telecom region in 3C-SiC,[206] with an optical transition lifetime less than 1 ns, room temperature operation, and high saturation count rate has been studied, however, the unknown origin not related to known defects, but rather to exciton recombination process of electrons and holes, the unknown spectral broadening can limit its application in quantum technologies. Array of nitrogen-vacancy $N_CV_{Si}^{(-)}$ were created and room temperature SPS demonstrated,[119118] showing full emission and excitation polarization for on-axis emitters and a high single-photon purity. A low-temperature SPS from shallow (100 nm from the surface) implanted neutral vanadium (V) was observed using in-resonance excitation[124] and its spectral

https://doi.org/10.1021/acsphotonics.1c01775
ACS Photonics 2022, 9, 1434−1457

stability assessed, showing the absence of spectral jumps with a 750 MHz line width (much larger that the lifetime limit ≈1 MHz), broadened by electrons and nuclear spins in the local environment.

From the point of view of SPSs, SiC has not yet achieved the same single-photon purity and indistinguishability of the current state of the art groups III−V quantum dots in micropillars.

In this respect, the current challenges are related mostly to defects spectral broadening due to doping and nanofabrication residual charge traps, however electrical and doping control together with passivation methods are available to reduce these effects and further increase the coupling, photon collection efficiency, and spin-coherence within a planar photonic crystal. One of the main open problems of SiC SPSs is the yield of fabrication and accuracy in localization of the color centers by using current low energy focused ion beams[207] or laser writing techniques.[208,209] One of the clear advantages of SiC SPSs is in their optoelectronic properties used to control color centers,[34] ranging from electrical excitation, electrical spectral tuning and broadening control, as shown in currently achieved SiC quantum-LED.[210−212]

Collection Enhancement and Control. The high refractive index of SiC ($n \sim 2.6$) limits free-space out-coupling of the centers emission due to large total internal reflections at the bulk material/air interface. Micro- and nanophotonic structures are therefore essential for their application to quantum technology. We discuss here solid immersion lenses and nanopillars used to improve the collection efficiency of SPSs in SiC.

Solid Immersion Lenses and Nanopillars. In the past decade, nano- and micropillars are being used extensively for enhancing SPS for quantum emitters such as color centers in diamond and for some of the low brightness color centers in SiC such as the $V_{Si}^{(-)}$, $V_C V_{Si}^{(0)}$, and $N_C V_{Si}^{(-)}$[21,213] and erbium.[214] The primary goal is to improve the collection efficiency for detection of single emitters[21] and for quantum sensing applications in ensemble emitters.[213] The experimental fluorescence enhancement values observed compared to bulk are around a factor of 10 and at the most of 20, while numerical models generally predict a much higher enhancement, up to 100 to 200.[215] One of the challenges is the positioning of the emitters inside the nanopillars, as the maximum fluorescent enhancement is observed for pillar diameters approximately half of the emission wavelength and for the dipole positioned at about half wavelength from the top. Limiting factors are the emitters broad emission at room temperature, as the nanopillar enhancement is wavelength-dependent, and the dipole emission, which is generally out of plane.[215] Further enhancement could be achieved by adopting metal-dielectric pillar resonators.[216] In particular, out of plane dipoles coupled to nanopillars may in principle achieve a free space enhanced collection efficiency up to 40−60%, but their single fiber coupling performance may be not optimal as the nanopillars transmission mode does not overlap well with the propagation mode of a single-mode fiber. Other nanostructures could be used for improving single mode fiber collection efficiency such as optimized inverted nanocones.[217]

Solid immersion lenses are typically a good choice to limit the impact of total internal reflection. Solid immersion lenses have also used to enhance optical collection from $V_{Si}^{(-)}$ and a scalable method to fabricate them, based on resist reflow and etching, has been demonstrated,[22,45] while with a lower fluorescence enhancement compared to nanopillars.[21]

Integration in Electronic Devices: Charge-State Control and Spectral Stability. In contrast to diamond which hosts similar SPSs and spin-defects, SiC is a technologically mature semiconductor, with established recipes for growth, doping, and fabrication of power-electronics devices. Integration of quantum spintronics with microelectronic functionalities opens the way to novel opportunities not available in diamond. Integration of spin centers into the intrinsic region of a p-i-n diode, for example, enables deterministic control of the center different charge states, each with its unique spin and optical properties.[35,49] Similarly to previous experiments on NV centers in diamond,[218] this could be used, for example, to switch between a $S = 1$ spin state that allows interfacing to photons and nuclear spins, to transfer quantum states from a quantum network to the quantum memory, and an $S = 0$ state which, by removing coupling to nuclear spins, protects the quantum states from external noise transmitted through the electron spin. Electrical control of the charge state of single V_{Si} has been proven,[35] permitting to enhance electrically the photon emission rate and establishing a route to deterministically control the charge state. A recent experiment with VV[49] has shown that, when operating the p-i-n diode at cryogenic temperature, one can observe broad Stark-shift tuning (>850 GHz) of the spin-selective transitions in the ZPL and a >50× line width narrowing, close to the lifetime limit, by depleting charges from the environment. This is a crucial result to preserve the coherence of the spin-photon interface, since it removes requirements on the physical parameters of the wave functions of the spin centers to couple weakly to electric fields, which is hard to control. These capabilities are only available in a wide bandgap semiconductor such as SiC, that can support the high electric field required to deplete charges. Specifically in SiC, this occurs for an electric field ≈1 MV/m[49] if compared to 4H- and 6H-SiC, with a breakdown voltage of $2-4 \times 10^4$ MV/m, which is about 8× higher than Si and GaAs.[219]

Spin-Photon Interface. Networked approaches to quantum information processing, consisting of small quantum modules connected by photonic channels, are receiving considerable interest for quantum communication and computing. This paradigm, with quantum modules operating as quantum repeaters, can mitigate the issue of bit-rates decreasing exponentially with distance (due to optical losses) in quantum communication. Depending on the protocol to be used,[220] photons only have to travel half the distance of the network link, which greatly increases the success-per-attempt, and consequently the overall bit rate. On the other hand quantum repeaters comprise a memory, mitigating the requirement for a correlated arrival of photons on a beam splitter. A future Quantum Internet would cascade several quantum repeaters, leading to a subexponential decay of the bit-rate with distance and paving the way for global sharing of quantum information. In the field of quantum computing, networking small quantum processing units through noisy and nondeterministic photonic channels is one of the most promising approaches toward noisy intermediate-scale quantum (NISQ) machines,[221,222] potentially even stretching to fault-tolerance. While several designs are currently being explored, implementations based on interfacing photons to individual solid state spins[223] have been particularly successful due to the long spin coherence times that can be achieved in host materials with low nuclear spin concentrations.

The requirements for an on-chip integrated spin-photon quantum module are as follows:

https://doi.org/10.1021/acsphotonics.1c01775
ACS Photonics 2022, 9, 1434−1457

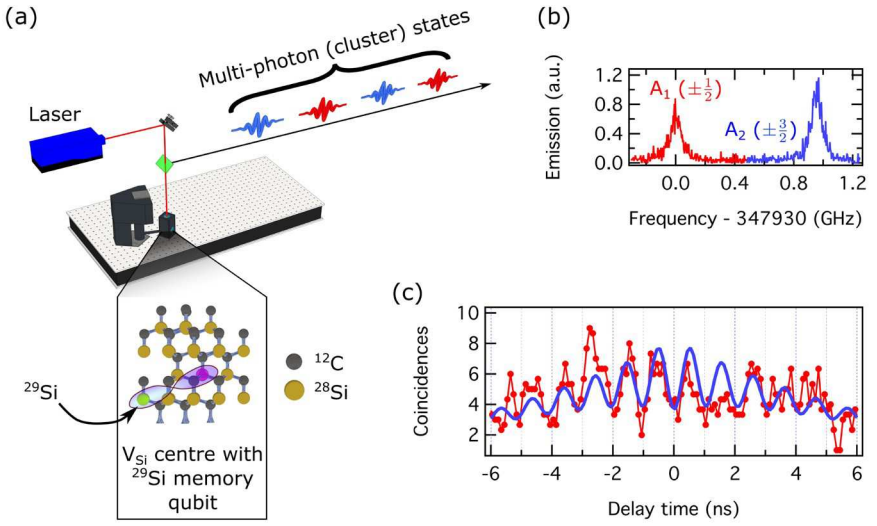

Figure 7. Spin-photon interfacing. (a) Schematic toward interfacing (frequency-encoded) photonic cluster states with spin-based quantum memories. The stationary multiqubit system comprises a single V_{Si} center in SiC, coupled to nearby nuclear spins, here indicated by a ^{29}Si spin. The V_{Si} center's robust spin-photon interface allows generation of multiphoton quantum states, for example, encoded in spectral-temporal modes. (b) Typical spectrum of a single V_{Si} center in high quality 4H-SiC. The two resonant emission lines in the ZPL are associated with spin-conserving transitions in the spin subspaces $m_s = \pm\frac{1}{2}$ (A_1) and $m_s = \pm\frac{3}{2}$ (A_2). Quite remarkably, nearly transform limited line widths are obtained, despite strong above-resonant excitation conditions. (c) Two-photon interference beat note in a Hong-Ou-Mandel-type experiment. Via coherent spin control, subsequently emitted photons have alternating color (as indicated in (a)). The beat note frequency equals the frequency difference between the A_1 and the A_2 optical transitions. Nonunity contrast is almost exclusively explained by nonideal spin manipulation. Image reprinted with permission from ref 36. Copyright 2020 Springer Nature under https://creativecommons.org/licenses/by/4.0/.

- An electronic spin with long coherence time, which can be initialized, manipulated, and readout (ideally in a single shot) with high fidelity. It should include the capabilities to address additional qubits, such as nearby nuclear spins to enable quantum error correction, entanglement purification, and quantum computational tasks.
- Coherent spin-photon interfacing requires spectrally stable, coherent spin-selective optical transitions, as close as possible to the lifetime limit. Photon distribution in (fiber) optical networks requires access to the O, C, and L telecom wavelength bands (1260−1360 and 1530−1625 nm). This may be achieved with systems that emit directly at those wavelengths or via noise-free quantum frequency conversion devices. The latter one could also be used advantageously to compensate wavelength differences among different emitters.[224]
- The possibility to develop a high-quality nanophotonic platform to enhance the light−matter interaction at the level of single quanta, for example, a deterministic (high-cooperativity) interaction between a single spin and a single photon without degrading the emitter optical and spin properties. In particular, optical cavities are required to increase photon generation rates and to improve collection efficiency. For an emitter coupled to a cavity, the spontaneous emission rate is enhanced and the lifetime is shortened by the Purcell factor $F_P \sim Q/V$, where Q is the cavity quality factor and V is the mode volume. Scalability considerations require this platform to embed all standard integrated photonic circuitry and to be fully compatible with industrial nanofabrication standards.

SiC provides long spin coherence time in a technologically mature platform, with several spin centers holding the promise to fulfill the requirements above. SiC is thus emerging as a viable material for the implementation of quantum spin-photon interface protocols[24,145] for remote entanglement and quantum networks,[24,31,36,225] quantum computing,[7,226] and quantum sensing.[35,41,43,45,107]

Resonant spin-photon interfacing has been studied extensively with the lower excited state manifolds of the V1 and V2 silicon vacancy (V_{Si}) centers in 4H-SiC.[24,36,39,145] The V1 (V2) optical emission is characterized by an excited state lifetime of 5−6 ns[133,134,141,145] and a ZPL peak at 862 nm (917 nm) with a Debye−Waller factor of 6−8% .[53,149] For both defects, optical transitions between the ground state and the lower excited state have been identified to be spin-conserving and linearly polarized.[24,145] As the spin states $m_s = \pm\frac{1}{2}$ and $m_s = \pm\frac{3}{2}$ are pairwise degenerate, a typical resonant absorption spectrum shows two distinct lines. They are labeled A_1 for the transition linking the $m_s = \pm\frac{1}{2}$ and A_2 for the $m_s = \pm\frac{3}{2}$ subspace, see Figure 7b. The spin-selectivity of the optical transitions has enabled high-contrast quantum state readout, while additional nonradiative decay channels involving metastable states show little spin selectivity and have thus been used for deterministic spin initialization with fidelities up to 97.5% .[24,145] In the perspective of developing quantum optical networks with V_{Si} centers, the rather strong coupling from the excited to the metastable states leads to a low cyclicity of the optical transitions ($\leq$10), which may be detrimental toward achieving single-shot readout and the emission of multiphoton states. However, this issue can be solved with the successful integration of V_{Si} into nanophotonic resonators that enhance the optical emission rates far beyond the intersystem-crossing rates.

The combination of high-fidelity initialization and readout has subsequently allowed to observe coherent dipolar interactions between a single V1 V_{Si} center and a single weakly coupled ^{29}Si nuclear spin.[24] Subsequently, a waveguide-integrated V2 center

https://doi.org/10.1021/acsphotonics.1c01775
ACS Photonics 2022, 9, 1434−1457

was used to control two nearby ^{29}Si nuclear spins with gate fidelity well-above 90%.[38]

A particularly interesting property of V_{Si}^- centers in n-type SiC with low nitrogen concentration ($[N] \leq 2 \times 10^{13}$ cm^{-3}) is their excellent spectral stability at cryogenic temperatures, which is on-par with state-of-the-art inversion symmetry defects in diamond, that is, the measured line widths are near transform limited and free of spectral diffusion.[24,36] Initially, it has been suspected that this is due to a near-identical electron density in the V_{Si}^- center ground and lower excited states, which eliminates coupling to stray electric fields in an elegant fashion.[146] With this model, strong optical transitions are still achieved due to an alternating sign in the ground and excited wave functions. However, subsequent measurements showed that the absorption wavelength of V_{Si}^- centers can be tuned via electric fields[40,227] with tuning coefficients close to the one of NV centers in diamond. This, therefore, requires more thorough studies to explain the excellent spectral stability of V_{Si}^- centers. Regarding the short time-scale line width of V_{Si}^- centers, a sizable broadening was only observed at temperatures $T > 5$ K for V1 and $T > 20$ K for V2 due to acoustic phonon scattering with higher lying electronic states.[36,53]

Remarkably, Morioka et al. showed further that even high-power above-resonant excitation does not induce any degradation of optical properties.[36] They used repeated picosecond excitation pulses and collected consecutively emitted ZPLs photons, which were subsequently used in Hong-Ou-Mandel type experiments. They showed two-photon indistinguishability exceeding 90%, which is comparable to the quantum dot,[228,229] diamond,[230] and single-molecule platforms.[231] Additionally, they took advantage of the V_{Si} center's unique spin-photon relation to spin-control the color of consecutively emitted photon pairs with high fidelity (Figure 7c). This proved that V_{Si} centers provide a coherent interface for generation of spin-photon entanglement and multiphoton cluster states, encoded in the frequency and time domains. Moreover, additional spin-photon entanglement generation schemes have been proposed.[137,138] Combined with coherent multiqubit spin control,[24] the system possesses all the requirements toward generation of network-relevant highly entangled states comprising multiple stationary spin qubits and multiphoton (cluster) states[232] (Figure 7a). The remarkable spectral stability of V_{Si}^- centers makes them also a prime candidate for integration into nanofabricated devices[39,165] in which electric field fluctuations are usually more prominent than in pristine bulk crystals. In this regard, a recent work showed V_{Si} centers retain the excellent spin-optical properties even after defect generation using ion bombardment and after integration into nanophotonic waveguides.[38]

The successful integration of V_{Si} centers into resonant enhancement structures will be crucial toward their usability in quantum applications. On one side, such resonators can increase the Debye–Waller factor from 6 to 8% to several 10%, thus maximizing the chance that a spin-photon entanglement generation attempt is successful. This is particularly important for the generation of multiphoton cluster states where multiple successive attempts have to be successful. Additionally, resonant enhancement of the radiative channels is required to improve the cyclicity of the optical transitions toward achieving single-shot spin state readout.[233] In this regard, it shall be mentioned that one of the "built-in" features of V_{Si} centers in 4H-SiC seems to be the separation of the optical lines by close to 1 GHz.[38,141] This limits the maximum Purcell enhancements that can be achieved before the optical lines show spectral overlap.

Further, a scalable integration of V_{Si} centers into nanofabricated devices will likely require external spectral tuning mechanisms to precisely match the resonant emission lines and line widths of multiple emitters. In this regard, recent studies showed that V_{Si} centers possess a remaining electric field sensitivity, such that intense electric fields can be used to tune the emission lines by 200 GHz,[40,150] which exceeds the inhomogeneous spectral distribution by at least 1 order of magnitude.[24,36,153] In addition, Lukin et al. showed that, by modulating the electric field faster than the excited state lifetime, arbitrary spectral features could be engineered,[40] providing a powerful method to match spectral features not only with other V_{Si} centers, but also other different optically active quantum systems in a hybrid quantum network.

At the same time, it should be noted that a successful integration of V_{Si} centers into resonant enhancement structures seems to be critical in order to increase fluorescence rates and single-shot spin state readout fidelity for application-relevant tasks. In this sense, significant lifetime shortenings have already been observed for V1′ centers integrated in photonic crystal cavities. So far, cavity experiments have focused only on the emission from the higher excited state manifold of V1′,[39,140] for which spin-selective excitation has not yet been demonstrated. Future research will be outlined to enhance the emission from the lower-lying V1 and V2 excited state manifolds.

Network-relevant SiC spin-photon interfaces are also available using divacancy centers. Their energy level structure is similar to NV centers in diamond,[157] which allows them to take advantage of well-established protocols and routines, and novel system-specific protocols have been proposed.[234] The use of divacancy centers may even appear favorable compared to NV centers in diamond, considering their near-telecom emission wavelength and the higher cyclicity of the optical transitions.[157] Divacancies have already been integrated into nanophotonic structures, achieving a Purcell enhancement of about 50 with an impressive increase of the DWF from 5% to 75%.[20] Although in these first nanostructures, narrow line widths have not been reported, several improvements can be made in the SiC host material, defect generation, and reduction of crystal damage during nanofabrication. It may also be interesting to combine these cavity structures with p-i-n diodes to reduce optical line widths.[49] While resonantly enhanced emission from divacancies will eventually lead to single-shot spin state readout, this milestone has already been achieved using optically induced spin-to-charge conversion.[9] In this scheme, photoionization of a single VV from the neutral (spin $S = 1$) charge state to its negative and dark charge state, enables mapping the defect spin to the charge state, that can be read-out with a fidelity of 80% in a single-shot and without the need of a photonic cavity.[9] The negative charge state of the VV is dark, and as such, if the spin state is prepared in the $m_s = 0$, by probing the defect with a 1131 nm in resonance excitation, no emission is observed. The process is possible because resonance excitation at 1131 nm of the neutral VV can initialize the spin in the $m_s = 0$ via selective spin transitions and a nonradiative transition to a metastable state, while it is not sufficient to induce charge conversion. When combined with a red-shifted 1151 nm excitation, the defect is converted into to its dark state via a two-photon process. This work by Anderson et al.[9] also demonstrated a record electron spin coherence time of 5 s, placing the divacancy in a leading position for entanglement distribution in quantum network or

https://doi.org/10.1021/acsphotonics.1c01775
ACS Photonics 2022, 9, 1434–1457

for ultrahigh sensitivity magnetic sensing. The demonstration of small quantum information processing units, for example, based on multiple long-coherence nuclear spins, requires the capability to control additional qubits. Protocols to control weakly coupled nuclear spins through dynamical decoupling sequences on the electronic spin, initially demonstrated for NV centers in diamond, have recently been extended to the VV in SiC.[226] As divacancies can be operated at elevated temperature up to $T = 10$ K before experiencing degradation of optical coherence,[157] multinuclear spin registers should be addressable using standard cryogenic equipment without any heating issues associated with microwave and radio frequency control. Overall, V_{Si} and divacancy centers show very promising features that may be relevant for the development of next-generation spin-photon interfaces for quantum network tasks. For both systems, nanointegration has demonstrated first successful results, and near-term research will focus on system integration into photonic crystal resonators while maintaining spin-optical coherence.

Quantum Sensing. Due to their long spin coherence times at room temperature and near-infrared emission, V_{Si} centers have been predicted to be a viable candidate for quantum sensing.[235] A key feature of V_{Si} centers is that when used in ensemble all align with the same magnetic dipole orientation (along the crystal *c*-axis),[129,136] in contrast for example to NV centers in diamond, which can be oriented along four different axes. This greatly enhances the ODMR contrast and thus the sensitivity. However, recent research has also identified various other promising candidates, such as the VV center and stacking fault related color centers.[236] Their higher spin contrast can compensate for the fact that those centers occur along multiple orientations.

SiC photonics is essential in quantum sensing applications to enhance the final sensitivity of the devices, for example by improving light extraction from the material using, for example, nanopillars[237] or if integrated in a cavity to improve the ODMR contrast, for example, for the optical in resonance excitation of the V1 line in the V_{Si}.[24] It is expected that SiC photonics integration will play a relevant role also in quantum sensing[238] by the enhancement of the signal-to-noise ratio of the optical spin read-out achieved, for example, by a 2D photonic crystal cavity into resonance with the color centers ZPL,[239] to enhance the overall sensitivity by increasing coupling to a single mode fiber, to increase speed and magnetic imaging resolution. Photonic cavities can advance quantum sensing at cryogenic temperatures, and a recent study suggests that the VV spin properties are maintained at low temperature.[240] Cryogenic sensors are currently needed in sectors such as aerospace, defense, energy, and scientific research for sensing fluids at cryogenic temperatures.[241]

Due to the demonstrated biocompatibility of SiC,[242] one the applications is in biological sensing. In this regard, SiC nanoparticles with spin defects can play a relevant role for enhanced sensitivity and high localization. Efforts are ongoing to study SiC nanoparticles hosting color centers. Using synchrotron-based Bragg coherent X-ray diffraction it has been shown that in SiC nanoparticles annealing reduces the strain due to the formation of the various spin defects such as the V_{Si} and the VV.[243] In addition, SiC nanoparticles as small as 3 nm have shown room temperature ODMR of the VV with a contrast of 3.5%, paving the way for novel spin sensing nanoprobes.[244] This combined with superesolution imaging[245] could advance current spin nanoscopy or nanomagnetic resonance imaging methods.

Sensing Magnetic Fields. Magnetic field sensing is typically based on measuring the shift of various energy levels in the presence of an external magnetic field. The most common approaches rely on spin-dependent fluorescence emission rates and controlled mixing of spin populations via microwave drive.[131,246−249] In this respect, one main challenge for single V_{Si} center is the rather low spin-dependent optical fluorescence contrast and the comparably dim photo emission.[41−46] Although some improvements have been achieved by integrating V_{Si} centers into nanopillars,[21] sensing schemes are still limited to DC magnetic field measurements. Ensemble-based sensors achieve sensitivities in optically detected magnetic resonance schemes of $\sim 10\ \mu T \cdot \sqrt{Hz}^{-1}$.[42] It is projected that improvements in spin manipulation techniques and isotopically engineered SiC samples can improve the sensitivity to $\sim 300\ nT/\sqrt{N} \cdot \sqrt{Hz}^{-1}$, with N being the number of active defects in the ensemble. A sensitivity of $50\ nT \cdot \sqrt{Hz}^{-1}$ was recently achieved.[250]

To improve on those results, other SiC color centers are studied. Room-temperature ODMR has been observed for PL1 (*hh*)[251] VV, with spin contrast ∼4%. VV configurations close to stacking faults (PL5−7 centers)[236] feature high ODMR contrast on the order of 20−25% and good photon emission rates,[251] which is comparable to NV centers in bulk diamond. Very recently, an unidentified center in SiC was created by carbon irradiation and high temperature annealing (1300°). It shows a prominent ZPL at 1007 nm and ODMR at room temperature.[126] $N_C V_{Si}^{(-)}$ centers in SiC also feature a room-temperature ODMR signal, albeit with low contrast.[119] One common advantage of all these centers is their near-infrared emission wavelength, which could play a quite significant role in magnetic sensing for biological applications due to the higher transparency of biological tissue compared to the visible range.[52]

Ensemble-based ODMR techniques require homogeneous spin manipulation throughout the entire sensor volume. Usually, this requires designing complex microwave antennas and/or shaping microwave drive pulses using optimal control algorithms.[252,253] The need for microwave drive was completely removed by taking advantage of the piezo-electric properties of SiC in order to drive spins with acoustic waves.[254] Another microwave-free approach was demonstrated by Simin et al., who reported all-optical magnetic field sensing with V_{Si} centers in isotopically purified 4H-SiC.[255] The scheme requires a well-adjusted offset magnetic field, such that the defects are operated at a spin level anticrossing. At this point, close to 100% fluorescence contrast was observed for small changes in the magnetic field. Initial field sensitivities of $\sim 100\ nT \cdot \sqrt{Hz}^{-1}$ are projected to be improved by 6 orders of magnitude using light-trapping waveguides. Remarkably, this sensing scheme was demonstrated for temperatures in excess of $T = 500$ K, which promises robust quantum sensors in harsh environments and space applications. Moreover, SiC hosts a large variety of defects covering zero field splitting (ZFS) from a few MHz to several GHz[128] and multiple "quantum-grade" polytypes can be stacked together.[106,201] This makes it possible to develop a multidefect sensor that covers a wide range of offset magnetic fields, thus further increasing the area of applications.

A major challenge associated with optical sensing schemes is that the signal quality is directly limited by the sensor's optical

https://doi.org/10.1021/acsphotonics.1c01775
ACS Photonics 2022, 9, 1434−1457

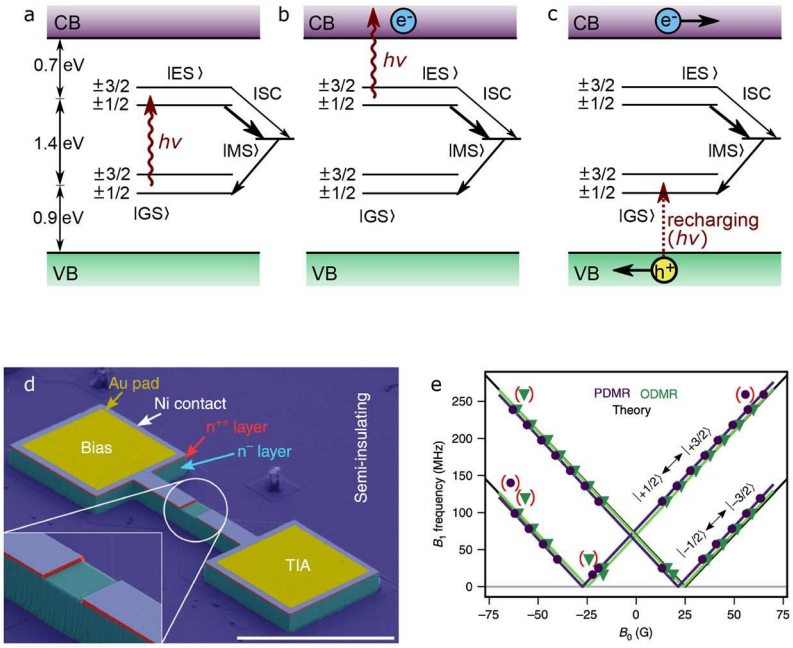

Figure 8. Magnetic field sensor based on PDMR with V_{Si} centers in 4H-SiC. (a) Relevant energy level scheme of V_{Si} centers. Spin-conserving optical excitation from the ground state (GS) to the excited state (ES) is indicated by a red arrow. Spin-dependent intersystem crossing occurs via metastable states (MS). (b) Upon two-photon absorption, the system is ionized and loses its electron to the conduction band (CB). (c) The system can return to its original charge state by capturing an electron from the valence band (VB), leaving a hole. The electron−hole pair can be separated, leading to a photocurrent. (d) SEM image of the sensing device (false color coded). The zoom-in shows the relevant sensing area, which has been etched to obtain an optical opening. (e) Comparison of traditional ODMR and PDMR Zeeman splitting signals, showing a near-perfect overlap. Image reprinted with permission from ref 47. Copyright 2019 Springer Nature under https://creativecommons.org/licenses/by/4.0/.

detection efficiency. Optical power loss is due to Fresnel reflection at the SiC crystal surface, material absorption, and limited light collection efficiency. In addition, especially for near-infrared emitters in SiC, photodetector efficiency is generally fairly low. At this point, the semiconductor properties of SiC can demonstrate their unique potential and strengths. Recent work demonstrated room-temperature photoelectric detection of magnetic resonance (PDMR).[47] As shown in Figure 8a−c, the technique relies on spin-dependent photoionization processes, that is, upon two-photon optical excitation, a color center may lose one electron to the conduction band, and subsequently return to its original charge state by capturing an electron from the valence band. The created electron−hole pair is then converted to an electrical current in a metal−semiconductor-metal junction, and directly measured after an on-chip transimpedance amplifier (see Figure 8d). So far, the principal functionality of the scheme was demonstrated (Figure 8e), and future research will be outlined to boost the sensitivity beyond previous diamond-based concept studies.[256−258]

Further steps toward ultra compact and robust sensors have been pioneered by Cochrane et al., who demonstrated electrically detected magnetic resonance (EDMR) close to zero magnetic fields.[259] The sensor is based on measuring changes in the electric current in a SiC p−n junction. Early demonstrations with a sensor setup covering only about 1 cm^3 showed a sensitivity of 440 $nT\cdot\sqrt{Hz}^{-1}$, and further optimizations are predicted to result in ∼1 $nT\cdot\sqrt{Hz}^{-1}$.

Sensing Temperature, Strain, and Electric Fields. Due to their infrared optical emission, thermometry with nanoscale color centers in SiC holds great promise for in situ monitoring of biological intracellular processes. Traditional schemes are based on measuring a temperature-dependent change in the ground and excited state ZFS. Kraus et al. demonstrated that Frenkel pairs (V_{Si}−Si_i) show a ground state ZFS shift of up to −1.1 MHz/K, which can be directly observed in ODMR experiments.[42] On the other hand, V_{Si} centers in SiC show a significant temperature-dependent change in the excited-state ZFS. Initial experiments inferred the ZFS by applying external magnetic fields in order to identify the anticrossing at which a change in fluorescence emission is observed.[51,52] Furthermore, recent low-temperature experiments on V_{Si} centers in high-quality SiC showed that the temperature-dependent excited-state ZFS can be inferred directly by measuring the optical absorption line separation of the spin-dependent transitions.[53] As the ground and excited state *g*-factors of V_{Si} centers are identical,[24] the optical line separation is not affected by magnetic fields, such that the method can be applied in arbitrary external magnetic fields. An interesting feature of V_{Si} centers is that their ground state ZFS is insensitive to temperature changes, thus permitting to implement a sensor that can unambiguously and independently infer both temperature and magnetic fields.

Electric field and strain sensing with color centers is traditionally based on inferring ZFS shifts, which are usually more prominent in the excited state manifolds. Both V_{Si} centers[40,56] and divacancy centers in SiC can be used for sensing electric and strain fields, however, the latter shows much higher sensitivity (up to twice as much as NV centers in diamond), which makes them preferable for those measurements. By measuring changes in the absorption line frequencies and ground state ZFS of divacancy centers, Falk et al. implemented strain and electric field sensors.[260] Microscopic electric field and strain sensors have been subsequently realized using VV and V_{Si} centers in 4H-SiC. The demonstrated methods use the fact that the fluorescence emission pattern of any defect

https://doi.org/10.1021/acsphotonics.1c01775
ACS Photonics 2022, 9, 1434−1457

depends strongly on its electronic charge environment, which influences the wave functions of the ground and excited states. By measuring the related energy level shifts, one can then gain access to the microscopic electronic (and strain) environment and the available electron density. To control and readout the charge state, all-optical schemes are sufficient,[35,54,55] resulting in sensitivities of $41 \pm 8\ (\mathrm{V/cm})^2 \cdot \sqrt{\mathrm{Hz}}^{-1}$ for AC electric fields.[261]

Additionally, another method for 2D vector electric field sensing with sensitivities down to 1 V/cm. The method takes advantage of the fact that VV centers exhibit bright and dark fluorescence emission depending on their charge state (neutral or negative). Using Electrometry by Optical Charge Conversion (EOCC) to dynamically control the charge state of VV centers, in conjunction with homodyne detection schemes, Wolfowicz et al. demonstrated that the rate of photoinduced charge conversion is sensitive to electric fields.[50] A likely explanation for this phenomenon are changes in the various ionization and capture cross sections of the defect.

CONCLUSIONS AND OUTLOOK

In this section, we give a brief outlook about what the current research challenges are for the field of SiC classical and quantum photonics, in particular, with respect to integrated photonics, single photon sources, spin-photon interfacing, and quantum sensing.

Photonic Technologies. While SiC has been for many years a material mostly used for power electronics applications, its excellent optical properties are currently being harnessed to develop photonic components. The main limitation toward large-scale photonic integrated circuits in SiC is the difficulty to obtain optical-grade thin membranes with minimal roughness, low absorption and uniform thickness across a large area. As we have discussed, a promising route being taken by different groups is to develop large-scale, high-quality SiC on insulator (SiCOI), though different techniques such as smart-cut or wafer bonding/thinning. SiCOI obtained by these techniques has already been used to fabricate high quality photonic resonators for classical PIC. For SiCOI fabricated using the smart-cut technique, the quality factor of resonators is limited to 10^6 unloaded and 10^4 when spin defects are integrated. This is currently in-par with other platforms such as diamond in regards to spin defects integration.[165]

While this effort is at the moment mainly limited to academic research, recently SOITEC, a company commercializing SOI, has announced the fabrication of high-quality SiC wafers obtained with smart cut, to reduce the carbon footprint of growing SiC epilayers, applying the same approach as SOI.[262] It can be thus be foreseen that SiCOI production will soon be scaled up to an industrial level, providing a major boost to further development of photonic components.

Several types of nonlinear devices have been already demonstrated in SiCOI, in particular for frequency conversion, frequency comb generation and electro-optical modulation. An ongoing challenge is the integration of multiple components on the same chip, to deliver complete photonic circuits.

One interesting opportunity is the integration of photonics with electronics on the same platform. In particular, the utilization of CMOS electronics within integrated photonics is a key for further advances in PIC. This has in fact been one of the major element for the progress of Si PICs.[263] In a recent demonstration in Si the photonics-electronics integration enables electrical control of a coupled ultrahigh-quality-factor nanocavity system on a silicon chip, transferring the confined photons from one to another cavity.[264] A similar idea could be applied to SiC. In this respect the main advantage of SiC compared to Si would be the high breakdown voltage (which would enable for example larger frequency tuning ranges of resonators by applying larger electric fields), strong thermal conductivity, lower absorption, good thermal stability, and broadband transparency. In addition to electronics and photonics integration as in Si, SiC also promises spintronics integration and could stimulate other applications, for example, in neuromorphic computing.

Quantum Photonic Technologies. Given the recent advances in material growth and nanofabrication,[38,169] SiCOI[21,39,165] is uniquely placed for bridging the classical and quantum photonics gap for QPICs.

The SiCOI platform could offer the possibility to integrate quantum emitters that provide high-quality spin-photon interfaces and quantum memories, with electrical control of their emission frequency and their spectral stability. The quantum emitters could be embedded in high-quality resonators with high Purcell factor, to boost the fraction of radiation into the coherent zero-phonon line, usable for quantum interference experiments. The collected emission could then be guided through different on-chip photonic components providing nonlinear frequency conversion, electrical modulation and filtering. We therefore believe that SiCOI is uniquely positioned to enable all-integrated quantum information devices, where all processing is done on-chip.

Further progress could pave the way for future photonic spin-photon interface quantum networks architecture[265] and integrated photonic circuits.[266,267] Near-future developments will certainly focus on demonstrating several functionalities on one chip, such as generation of entanglement among multiple emitters in cavities via on-chip photonic interference, on-chip light generation and quantum frequency conversion, as well as on-chip integration of superconducting nanowire single photon detectors (SNSPDs).[268]

As for the classical applications described above, the integration of electronics with photonics could have a major impact for quantum technology, for example, for tuning the frequency of spin-selective optical transitions and preserving their spectral stability.[49] This capability is otherwise only available in the III−V platform,[269] which is, however, less appealing from the spintronics point of view due to short spin coherence times induced by a large concentration of nuclear spins.

Single Photon Sources. The visible SPSs in SiC are among the top brightest quantum emitters in any bulk material at room temperature, and their spectral emission should be further controlled either electrically or by passivation methods to achieve indistinguishability and frequency conversion for quantum communication applications.[23,202,203,210] Their full identification and charge state conversion should be pursued for applications in electrical control and detection. Due to the variety of possible quantum emitters in the visible in SiC, the challenges are to isolate and better determine the origin for their on demand engineering and control, particularly in nanocrystals of SiC.[200,244,270] While color centers are currently mainly investigated for QPIC, due to high nonlinear second and third order coefficients, SiC photonic cavities could be used to create quantum states of light based on spontaneuos parametric down-

https://doi.org/10.1021/acsphotonics.1c01775
ACS Photonics 2022, 9, 1434−1457

conversion (SPDC) and spontaneous four-wave mixing (SFWM) in SiC as an alternative quantum source of light.[84]

Spin-Photon Interface. Several challenges are still outstanding in relation to the implementation of spin-photon entanglement for future SiC-based quantum networking devices.

One of the challenges is the spectral stability of the spin-selective atomic-like optical transitions typically used for spin-photon interfacing. As SiC is a noncentrosymmetric crystal, it does not possess color centers with inversion symmetry (as for example group-IV vacancy systems in diamond), that are insensitive to electric fields by group theory considerations. As such, color centers in SiC are generally much more prone to spectral diffusion. However, single photon indistinguishability has been demonstrated using spin conserving transitions in the V_{Si}, and regardless of its low brightness, among all the color centers, it is one of the best candidates for spin-photon interface applications. The other challenge is material damage induced by the color centers creation and by photonic structures fabrication, which cannot be fully recovered by annealing within the temperature ranges where the desired color centers can survive. A crucial target is the creation of color centers with the same spin coherence properties of naturally occurring emitters, as well as their integration in photonic components, while preserving the same optical and spin properties they possess in pristine material. Integration of V_{Si} into a photonic structure, while preserving its spectral stability and spin coherence has been recently demonstrated together with quantum gates operation within photonic waveguides.[38] At the same time, the deterministic creation of the V_{Si} with the same spin and spectral properties as the as-grown emitters has been achieved.[38] Next steps will include more deterministic creation of color centers within photonic waveguide/cavities maintaining the high spectral stability and long spin coherence to achieve spin-photon entanglement, quantum operation and strong light matter interaction enabling single-shot read out and demonstration via coupled spin-photon interface 2D photons cluster states.[271]

To implement quantum communication networks single shot read-out and single mode coupling with high efficiency of the integrated color centers to fiber should be achieved. Single-shot spin readout is a key element to achieve entanglement distribution and quantum error correction, which are essential to practically realize quantum networks. Single-shot spin read out also provides an increased signal-to-noise ratio for quantum sensing.

Deterministic single-shot readout of individual electron spins in V_{Si}, regardless of the spin selective transition, may be difficult to achieve due to the absence of a highly cycling spin selective optical transition without spin-flips in the excited stated.

On the other hand, as discussed above, single-shot read-out has been achieved for the divacancy (VV) by using spin-to-charge conversion.[9] This spin read-out protocol also opens the opportunity to be extended to electrical detection, potentially bridging the gap between classical electric devices in SiC such as MOSFET and single-charge quantum devices.

Quantum Sensing. The current SiC photonics technology is already capable of being utilized to enhance the signal-to-noise ratio, integration, and sensitivity of future devices for quantum sensing: specifically for magnetic sensing due to the special dipole orientation of the V_{Si} or the very long coherence time of up to 5 s of the divacancy.[9] As an example, all-optical magnetic sensing in SiC photonic confinement could achieve up to 6 orders of magnitude improvement of the current sensitivity of 100 nT/$\sqrt{\text{Hz}}$.[255] Some of the remaining challenges are the fluorescence enhancement of color centers emission into single mode fibers and waveguides. Alternatively SiC can offer electrical read out of the spin under all-optical excitation in harsh environment. SiC photonics could in particular enhance electric and temperature sensing due to the material more favorable emission dependence on temperature and electric fields. Finally, the recent discovery of stimulated emission associated with single VV[9] and their spin transition could be utilized in the laser-threshold magnetometry promising pT/$\sqrt{\text{Hz}}$ sensitivity.[272] Another approach for increasing the spin read-out contrast for magnetometry in SiC defects such as VV, could be based on achieving strong coupling in high-Q macroscopic microwave cavities,[273,274] which has recently shown a 97% ODMR contrast of ensemble of NV center in diamond microwave read-out and few pT/$\sqrt{\text{Hz}}$ sensitivity at room temperature.[275]

Other Quantum Photonic Technologies. Further improvements in the fabrication of nanocavities with high quality factors and small mode volumes, combined with the advances in color center integration, will lead to cavity quantum electrodynamic effects in the strong coupling regime.[276] Here, light−matter interaction has an intensity that overcomes the losses to the environment. Multiemitter cavity systems have also been proposed as a path to reaching this regime.[277] Here, the ideal platforms would be the ones with little to no strain unaffected by inhomogeneous broadening, such as those recently demonstrated in triangular SiC devices.[38] The emergent polaritonic physics of strongly coupled systems will have applications in quantum light generation,[278,279] quantum simulation,[280,281] and low-power optical switching.[282] By using weakly pumped FWM, heralded single photons and energy-time entangled pairs can be generated. Recently using FWM in SiC integrated ring resonators, the quantum optics of the soliton microcomb has been studied,[84] paving the way for multimode quantum resource using optical combs.[283]

AUTHOR INFORMATION

Corresponding Author

Stefania Castelletto − *School of Engineering, RMIT University, Melbourne, Victoria 3001, Australia;* orcid.org/0000-0002-8675-2291; Email: stefania.castelletto@rmit.edu.au

Authors

Alberto Peruzzo − *Quantum Photonics Laboratory and Centre for Quantum Computation and Communication Technology, School of Engineering, RMIT University, Melbourne, Victoria 3001, Australia;* orcid.org/0000-0002-7953-3875

Cristian Bonato − *Institute of Photonics and Quantum Sciences, SUPA, Heriot-Watt University, Edinburgh EH14 4AS, United Kingdom*

Brett C. Johnson − *Quantum Photonics Laboratory and Centre for Quantum Computation and Communication Technology, School of Engineering, RMIT University, Melbourne, Victoria 3001, Australia*

Marina Radulaski − *Department of Electrical and Computer Engineering, University of California, Davis, California 95616, United States;* orcid.org/0000-0001-9606-3716

Haiyan Ou − *DTU Fotonik, Technical University of Denmark, DK-2800 Kongens, Lyngby, Denmark;* orcid.org/0000-0002-0538-8230

https://doi.org/10.1021/acsphotonics.1c01775
ACS Photonics 2022, 9, 1434−1457

Florian Kaiser − *3rd Institute of Physics, IQST, and Research Center SCoPE, University of Stuttgart, 70569 Stuttgart, Germany*

Joerg Wrachtrup − *3rd Institute of Physics, IQST, and Research Center SCoPE, University of Stuttgart, 70569 Stuttgart, Germany*

Complete contact information is available at: https://pubs.acs.org/10.1021/acsphotonics.1c01775

Funding

A.P. is funded by RMIT University Vice-Chancellor's Senior Research Fellowship, by a Google Faculty Research Award and by the Australian Government through the Australian Research Council under the Centre of Excellence Scheme No. CE170100012. C.B. is funded by the Engineering and Physical Sciences Research Council (EP/S000550/1 and EP/V053779/1), the Leverhulme Trust (RPG-2019-388), and the European Commission (QuanTELCO, Grant Agreement No. 862721). F.K. and J.W. are funded by the European Research Council (ERC) Grant SMel, the European Commission Marie Curie ETN "QuSCo" (Grant Agreement No. 765267), the Max Planck Society, the Humboldt Foundation, and the German Research Foundation (SPP 1601), the German Federal Ministry of Education and Research (BMBF) with the Projects Q.Link.X (Grant Agreement No. 16KIS0867), QR.X (Grant Agreement No. 16KISQ013), QVOL (Grant Agreement No. 03ZU1110IB), and Spinning (Grant Agreement No. 13N16219), the Ministerium für Wirtschaft, Arbeit and Tourismus Baden-Württemberg with the Projects SPOC (Grant Agreement No. QT-6) and QC4BW (Grant Agreement No. 3-4332.62-IAF/7), as well as the EU-FET Flagship on Quantum Technologies through the Projects ASTERIQS (Grant Agreement ID: 820394) and QIA (Grant Agreement ID: 820445). H.O. is funded by the EU Horizon 2020 Research and Innovation Program FET Open through the Project SiComb (Grant Agreement No. 899679). M.R. is funded by the National Science Foundation CAREER Award 2047564.

Notes

The authors declare no competing financial interest.

REFERENCES

(1) Eddy, C. R.; Gaskill, D. K. Silicon Carbide as a Platform for Power Electronics. *Science* **2009**, *324*, 1398−1400.

(2) Bhatnagar, M.; Baliga, B. J. Comparison of 6H-SiC, 3C-SiC, and Si for power devices. *IEEE Trans. Electron Devices* **1993**, *40*, 645−655.

(3) Matsunami, H. Current SiC technology for power electronic devices beyond Si. *Microelectron. Eng.* **2006**, *83*, 2−4.

(4) Ding, X.; Du, M.; Zhou, T.; Guo, H.; Zhang, C. Comprehensive comparison between silicon carbide MOSFETs and silicon IGBTs based traction systems for electric vehicles. *Appl. Energy* **2017**, *194*, 626−634.

(5) Leijtens, X. JePPIX: the platform for Indium Phosphide-based photonics. *IET Optoelectron* **2011**, *5* (4), 202−206.

(6) Lohrmann, A.; Johnson, B.; McCallum, J.; Castelletto, S. A review on single photon sources in silicon carbide. *Rep. Prog. Phys.* **2017**, *80*, 034502.

(7) Atatüre, M.; Englund, D.; Vamivakas, N.; Lee, S.-Y.; Wrachtrup, J. Material platforms for spin-based photonic quantum technologies. *Nat. Rev. Mater.* **2018**, *3*, 38−51.

(8) Son, N. T.; Anderson, C. P.; Bourassa, A.; Miao, K. C.; Babin, C.; Widmann, M.; Niethammer, M.; Ul Hassan, J.; Morioka, N.; Ivanov, I. G.; Kaiser, F.; Wrachtrup, J.; Awschalom, D. D. Developing silicon carbide for quantum spintronics. *Appl. Phys. Lett.* **2020**, *116*, 190501.

(9) Anderson, C. P.; Glen, E. O.; Zeledon, C.; Bourassa, A.; Jin, Y.; Zhu, Y.; Vorwerk, C.; Crook, A. L.; Abe, H.; Ul-Hassan, J.; Ohshima, T.; Son, N. T.; Galli, G.; Awschalom, D. D. Five-second coherence of a single spin with single-shot readout in silicon carbide. *Sci. Adv.* **2022**, *8*, No. eabm5912.

(10) Simin, D.; Kraus, H.; Sperlich, A.; Ohshima, T.; Astakhov, G. V.; Dyakonov, V. Locking of electron spin coherence above 20 ms in natural silicon carbide. *Phys. Rev. B Condens. Matter.* **2017**, *95*, 161201.

(11) Yang, L. P.; Burk, C.; Widmann, M.; Lee, S. Y.; Wrachtrup, J.; Zhao, N. Electron spin decoherence in silicon carbide nuclear spin bath. *Phys. Rev. B: Condens. Matter.* **2014**, *90*, 1−6.

(12) Kanai, S.; Heremans, F. J.; Seo, H.; Wolfowicz, G.; Anderson, C. P.; Sullivan, S. E.; Onizhuk, M.; Galli, G.; Awschalom, D. D.; Ohno, H. Generalized scaling of spin qubit coherence in over 12,000 host materials. *Proc. Natl. Acad. Sci. U.S.A.* **2022**, *119*, na.

(13) Zhang, G.; Cheng, Y.; Chou, J.-P.; Gali, A. Material platforms for defect qubits and single-photon emitters. *Appl. Phys. Rev.* **2020**, *7*, 031308.

(14) Castelletto, S. Silicon carbide single-photon sources: challenges and prospects. *Materials for Quantum Technology* **2021**, *1*, 023001.

(15) Kues, M.; Reimer, C.; Lukens, J. M.; Munro, W. J.; Weiner, A. M.; Moss, D. J.; Morandotti, R. Quantum optical microcombs. *Nat. Photonics* **2019**, *13*, 170−179.

(16) Liu, L.; Zhao, J.; Cao, G.; Zheng, S.; Yan, X. A Memristor-Based Silicon Carbide for Artificial Nociceptor and Neuromorphic Computing. *Adv. Mater. Technol.* **2021**, *6*, 2100373.

(17) Majety, S.; Norman, V. A.; Li, L.; Bell, M.; Saha, P.; Radulaski, M. Quantum photonics in triangular-cross-section nanodevices in silicon carbide. *JPhys. Photonics* **2021**, *3*, 034008.

(18) Chatzopoulos, I.; Martini, F.; Cernansky, R.; Politi, A. High-Q/V photonic crystal cavities and QED analysis in 3C-SiC. *ACS Photonics* **2019**, *6*, 1826−1831.

(19) Guidry, M. A.; Yang, K. Y.; Lukin, D. M.; Markosyan, A.; Yang, J.; Fejer, M. M.; Vučković, J. Optical parametric oscillation in silicon carbide nanophotonics. *Optica* **2020**, *7*, 1139−1142.

(20) Crook, A. L.; Anderson, C. P.; Miao, K. C.; Bourassa, A.; Lee, H.; Bayliss, S. L.; Bracher, D. O.; Zhang, X.; Abe, H.; Ohshima, T.; Hu, E. L.; Awschalom, D. D. Purcell Enhancement of a Single Silicon Carbide Color Center with Coherent Spin Control. *Nano Lett.* **2020**, *20*, 3427−3434.

(21) Radulaski, M.; Widmann, M.; Niethammer, M.; Zhang, J. L.; Lee, S.-Y.; Rendler, T.; Lagoudakis, K. G.; Son, N. T.; Janzen, E.; Ohshima, T.; et al. Scalable quantum photonics with single color centers in silicon carbide. *Nano Lett.* **2017**, *17*, 1782−1786.

(22) Sardi, F.; Kornher, T.; Widmann, M.; Kolesov, R.; Schiller, F.; Reindl, T.; Hagel, M.; Wrachtrup, J. Scalable production of solid-immersion lenses for quantum emitters in silicon carbide. *Appl. Phys. Lett.* **2020**, *117*, 022105.

(23) Castelletto, S.; Johnson, B. C.; Ivády, V.; Stavrias, N.; Umeda, T.; Gali, A.; Ohshima, T. A silicon carbide room-temperature single-photon source. *Nat. Mater.* **2014**, *13*, 151−156.

(24) Nagy, R.; et al. High-fidelity spin and optical control of single silicon-vacancy centres in silicon carbide. *Nat. Commun.* **2019**, *10*, 1954.

(25) Guo, X.; Peng, Z.; Ding, P.; Li, L.; Chen, X.; Wei, H.; Tong, Z.; Guo, L. Nonlinear optical properties of 6H-SiC and 4H-SiC in an extensive spectral range. *Opt. Mater. Express* **2021**, *11*, 1080−1092.

(26) Liu, X.; Shimada, T.; Miura, R.; Iwamoto, S.; Arakawa, Y.; Kato, Y. K. Localized guided-mode and cavity-mode double resonance in photonic crystal nanocavities. *Phys. Rev. Applied* **2015**, *3*, 014006.

(27) Lu, W.; Ou, Y.; Fiordaliso, E. M.; Iwasa, Y.; Jokubavicius, V.; Syväjärvi, M.; Kamiyama, S.; Petersen, P. M.; Ou, H. White light emission from fluorescent SiC with porous surface. *Sci. Rep.* **2017**, *7*, 1−9.

(28) Iwamoto, N.; Svensson, B. G. In *Defects in Semiconductors*; Semiconductors and Semimetals; Romano, L., Privitera, V., Jagadish, C., Eds.; Elsevier, 2015; Vol. *91*; pp 369−407.

(29) Yi, A.; Zheng, Y.; Huang, H.; Lin, J.; Yan, Y.; You, T.; Huang, K.; Zhang, S.; Shen, C.; Zhou, M.; Huang, W.; Zhang, J.; Zhou, S.; Ou, H.;

Ou, X. Wafer-scale 4H-silicon carbide-on-insulator (4H-SiCOI) platform for nonlinear integrated optical devices. *Opt. Mater.* **2020**, *107*, 109990.
(30) Fan, T.; Moradinejad, H.; Wu, X.; Eftekhar, A. A.; Adibi, A. High-Q integrated photonic microresonators on 3C-SiC-on-insulator (SiCOI) platform. *Opt. Express* **2018**, *26*, 25814−25826.
(31) Awschalom, D. D.; Hanson, R.; Wrachtrup, J.; Zhou, B. B. Quantum technologies with optically interfaced solid-state spins. *Nat. Photonics* **2018**, *12*, 516−527.
(32) Bathen, M. E.; Vines, L. Manipulating Single-Photon Emission from Point Defects in Diamond and Silicon Carbide. *Adv. Quantum Technol.* **2021**, *4*, 2100003.
(33) Khramtsov, I. A.; Fedyanin, D. Y. Single-Photon Sources Based on Novel Color Centers in Silicon Carbide P−I−N Diodes: Combining Theory and Experiment. *Nano-Micro Lett.* **2021**, *13*, 1−12.
(34) Fedyanin, D. Y. Optoelectronics of Color Centers in Diamond and Silicon Carbide: From Single-Photon Luminescence to Electrically Controlled Spin Qubits. *Adv. Quantum Technol.* **2021**, *4*, 2100048.
(35) Widmann, M.; et al. Electrical Charge State Manipulation of Single Silicon Vacancies in a Silicon Carbide Quantum Optoelectronic Device. *Nano Lett.* **2019**, *19*, 7173−7180.
(36) Morioka, N.; et al. Spin-controlled generation of indistinguishable and distinguishable photons from silicon vacancy centres in silicon carbide. *Nat. Commun.* **2020**, *11*, 1−8.
(37) Bourassa, A.; Anderson, C. P.; Miao, K. C.; Onizhuk, M.; Ma, H.; Crook, A. L.; Abe, H.; Ul-Hassan, J.; Ohshima, T.; Son, N. T.; Galli, G.; Awschalom, D. D. Entanglement and control of single nuclear spins in isotopically engineered silicon carbide. *Nat. Mater.* **2020**, *19*, 1319−1325.
(38) Babin, C.; Stöhr, R.; Morioka, N.; Linkewitz, T.; Steidl, T.; Wörnle, R.; Liu, D.; Hesselmeier, E.; Vorobyov, V.; Denisenko, A.; et al. Fabrication and nanophotonic waveguide integration of silicon carbide colour centres with preserved spin-optical coherence. *Nat. Mater.* **2022**, *21*, 67−73.
(39) Lukin, D. M.; Dory, C.; Guidry, M. A.; Yang, K. Y.; Mishra, S. D.; Trivedi, R.; Radulaski, M.; Sun, S.; Vercruysse, D.; Ahn, G. H.; Vučković, J. 4H-silicon-carbide-on-insulator for integrated quantum and nonlinear photonics. *Nat. Photonics* **2020**, *14*, 330−334.
(40) Lukin, D. M.; et al. Spectrally reconfigurable quantum emitters enabled by optimized fast modulation. *Npj Quantum Inf* **2020**, *6*, 1−9.
(41) Simin, D.; Fuchs, F.; Kraus, H.; Sperlich, A.; Baranov, P. G.; Astakhov, G. V.; Dyakonov, V. High-Precision Angle-Resolved Magnetometry with Uniaxial Quantum Centers in Silicon Carbide. *Phys. Rev. Applied* **2015**, *4*, 014009.
(42) Kraus, H.; Soltamov, V. A.; Fuchs, F.; Simin, D.; Sperlich, A.; Baranov, P. G.; Astakhov, G. V.; Dyakonov, V. Magnetic field and temperature sensing with atomic-scale spin defects in silicon carbide. *Sci. Rep.* **2015**, *4*, 5303.
(43) Niethammer, M.; Widmann, M.; Lee, S.-Y.; Stenberg, P.; Kordina, O.; Ohshima, T.; Son, N. T.; Janzén, E.; Wrachtrup, J. Vector Magnetometry Using Silicon Vacancies in 4*H*-SiC Under Ambient Conditions. *Phys. Rev. Applied* **2016**, *6*, 034001.
(44) Cochrane, C. J.; Kraus, H.; Neudeck, P. G.; Spry, D. J.; Waskiewicz, R. J.; Ashton, J. P.; Lenahan, P. M. Magnetic Field Sensing with 4H SiC Diodes: N vs P Implantation. *Silicon Carbide and Related Materials 2017* **2018**, *924*, 988−992.
(45) Widmann, M.; et al. Coherent control of single spins in silicon carbide at room temperature. *Nat. Mater.* **2015**, *14*, 164−168.
(46) Lee, S.-Y.; Niethammer, M.; Wrachtrup, J. Vector magnetometry based on $S = 3/2$ electronic spins. *Phys. Rev. B Condens. Matter.* **2015**, *92*, 115201.
(47) Niethammer, M.; Widmann, M.; Rendler, T.; Morioka, N.; Chen, Y.-C.; Stöhr, R.; Hassan, J. U.; Onoda, S.; Ohshima, T.; Lee, S.-Y.; Mukherjee, A.; Isoya, J.; Son, N. T.; Wrachtrup, J. Coherent electrical readout of defect spins in silicon carbide by photo-ionization at ambient conditions. *Nat. Commun.* **2019**, *10*, 5569.
(48) Miao, K. C.; Bourassa, A.; Anderson, C. P.; Whiteley, S. J.; Crook, A. L.; Bayliss, S. L.; Wolfowicz, G.; Thiering, G.; Udvarhelyi, P.; Ivády, V.; Abe, H.; Ohshima, T.; Gali, d.; Awschalom, D. D. Electrically driven optical interferometry with spins in silicon carbide. *Sci. Adv.* **2019**, *5*, No. eaay0527.
(49) Anderson, C. P.; Bourassa, A.; Miao, K. C.; Wolfowicz, G.; Mintun, P. J.; Crook, A. L.; Abe, H.; Hassan, J. U.; Son, N. T.; Ohshima, T.; Awschalom, D. D. Electrical and optical control of single spins integrated in scalable semiconductor devices. *Science* **2019**, *366*, 1225−1230.
(50) Wolfowicz, G.; Anderson, C. P.; Whiteley, S. J.; Awschalom, D. D. Heterodyne detection of radio-frequency electric fields using point defects in silicon carbide. *Appl. Phys. Lett.* **2019**, *115*, 043105.
(51) Anisimov, A. N.; Simin, D.; Soltamov, V. A.; Lebedev, S. P.; Baranov, P. G.; Astakhov, G. V.; Dyakonov, V. Optical thermometry based on level anticrossing in silicon carbide. *Sci. Rep.* **2016**, *6*, 2−6.
(52) Ohshima, T.; Satoh, T.; Kraus, H.; Astakhov, G. V.; Dyakonov, V.; Baranov, P. G. Creation of silicon vacancy in silicon carbide by proton beam writing toward quantum sensing applications. *J. Phys. D: Appl. Phys.* **2018**, *51*, 333002.
(53) Udvarhelyi, P.; Thiering, G.; Morioka, N.; Babin, C.; Kaiser, F.; Lukin, D.; Ohshima, T.; Ul-Hassan, J.; Son, N. T.; Vučković, J.; Wrachtrup, J.; Gali, A. Vibronic States and Their Effect on the Temperature and Strain Dependence of Silicon-Vacancy Qubits in 4H-Si C. *Phys. Rev. Applied* **2020**, *13*, 1−10.
(54) Wolfowicz, G.; Anderson, C. P.; Yeats, A. L.; Whiteley, S. J.; Niklas, J.; Poluektov, O. G.; Heremans, F. J.; Awschalom, D. D. Optical charge state control of spin defects in 4H-SiC. *Nat. Commun.* **2017**, *8*, 1876.
(55) Golter, D. A.; Lai, C. W. Optical switching of defect charge states in 4H-SiC. *Sci. Rep.* **2017**, *7*, 13406.
(56) Breev, I. D.; Poshakinskiy, A. V.; Yakovleva, V. V.; Nagalyuk, S. S.; Mokhov, E. N.; Hübner, R.; Astakhov, G. V.; Baranov, P. G.; Anisimov, A. N. Stress-controlled zero-field spin splitting in silicon carbide. *Appl. Phys. Lett.* **2021**, *118*, 084003.
(57) Wang, S.; Zhan, M.; Wang, G.; Xuan, H.; Zhang, W.; Liu, C.; Xu, C.; Liu, Y.; Wei, Z.; Chen, X. 4H-SiC: a new nonlinear material for midinfrared lasers. *Laser Photonics Rev.* **2013**, *7*, 831−838.
(58) Zheng, Y.; Pu, M.; Yi, A.; Ou, X.; Ou, H. 4H-SiC microring resonators for nonlinear integrated photonics. *Opt. Lett.* **2019**, *44*, 5784−5787.
(59) Zheng, Y.; Pu, M.; Yi, A.; Chang, B.; You, T.; Huang, K.; Kamel, A. N.; Henriksen, M. R.; Jørgensen, A. A.; Ou, X.; et al. High-quality factor, high-confinement microring resonators in 4H-silicon carbide-on-insulator. *Opt. Express* **2019**, *27*, 13053−13060.
(60) Yu, M.; Okawachi, Y.; Cheng, R.; Wang, C.; Zhang, M.; Gaeta, A. L.; Lončar, M. Raman lasing and soliton mode-locking in lithium niobate microresonators. *Light Sci. Appl.* **2020**, *9*, 1−7.
(61) Wilson, D. J.; Schneider, K.; Hönl, S.; Anderson, M.; Baumgartner, Y.; Czornomaz, L.; Kippenberg, T. J.; Seidler, P. Integrated gallium phosphide nonlinear photonics. *Nat. Photonics* **2020**, *14*, 57−62.
(62) Dutta, S.; Goldschmidt, E. A.; Barik, S.; Saha, U.; Waks, E. Integrated photonic platform for rare-earth ions in thin film lithium niobate. *Nano Lett.* **2020**, *20*, 741−747.
(63) Wu, I. J.; Guo, G. Y. Second-harmonic generation and linear electro-optical coefficients of SiC polytypes and nanotubes. *Phys. Rev. B: Condens. Matter.* **2008**, *78*, 35447.
(64) Martini, F.; Politi, A. Four wave mixing in 3C SiC ring resonators. *Appl. Phys. Lett.* **2018**, *112*, 251110.
(65) Sato, H.; Abe, M.; Shoji, I.; Suda, J.; Kondo, T. Accurate measurements of second-order nonlinear optical coefficients of 6H and 4H silicon carbide. *J. of the Opt. Society of America B* **2009**, *26*, 1892−1896.
(66) Hausmann, B.; Bulu, I.; Venkataraman, V.; Deotare, P.; Lončar, M. Diamond nonlinear photonics. *Nat. Photonics* **2014**, *8*, 369−374.
(67) Dinu, M.; Quochi, F.; Garcia, H. Third-order nonlinearities in silicon at telecom wavelengths. *Appl. Phys. Lett.* **2003**, *82*, 2954−2956.
(68) Liu, X.; Sun, C.; Xiong, B.; Wang, L.; Wang, J.; Han, Y.; Hao, Z.; Li, H.; Luo, Y.; Yan, J.; Wei, T.; Zhang, Y.; Wang, J. Aluminum nitride-on-sapphire platform for integrated high-Q microresonators. *Opt. Express* **2017**, *25*, 587−594.

https://doi.org/10.1021/acsphotonics.1c01775
ACS Photonics 2022, 9, 1434−1457

(69) Pu, M.; Ottaviano, L.; Semenova, E.; Yvind, K. Efficient frequency comb generation in AlGaAs-on-insulator. *Optica* **2016**, *3*, 823−826.
(70) Ikeda, K.; Saperstein, R. E.; Alic, N.; Fainman, Y. Thermal and Kerr nonlinear properties of plasma-deposited silicon nitride/silicon dioxide waveguides. *Opt. Express* **2008**, *16*, 12987−12994.
(71) Schiek, R. Absolute measurement of the quadratic nonlinear susceptibility of lithium niobate in waveguides. *Nonlinear Opt.* **2011**, NWE15.
(72) Xing, P.; Ma, D.; Ooi, K. J.; Choi, J. W.; Agarwal, A. M.; Tan, D. CMOS-compatible PECVD silicon carbide platform for linear and nonlinear optics. *ACS Photonics* **2019**, *6*, 1162−1167.
(73) Wang, C.; Fang, Z.; Yi, A.; Yang, B.; Wang, Z.; Zhou, L.; Shen, C.; Zhu, Y.; Zhou, Y.; Bao, R.; et al. High-Q microresonators on 4H-silicon-carbide-on-insulator platform for nonlinear photonics. *Light Sci. Appl.* **2021**, *10*, 1−11.
(74) Yamada, S.; Song, B.-S.; Jeon, S.; Upham, J.; Tanaka, Y.; Asano, T.; Noda, S. Second-harmonic generation in a silicon-carbide-based photonic crystal nanocavity. *Opt. Lett.* **2014**, *39*, 1768−1771.
(75) Song, B.-S.; Asano, T.; Jeon, S.; Kim, H.; Chen, C.; Kang, D. D.; Noda, S. Ultrahigh-Q photonic crystal nanocavities based on 4H silicon carbide. *Optica* **2019**, *6*, 991−995.
(76) Lu, X.; Lee, J. Y.; Feng, P. X.-L.; Lin, Q. High Q silicon carbide microdisk resonator. *Appl. Phys. Lett.* **2014**, *104*, 181103.
(77) De Leonardis, F.; Soref, R. A.; Passaro, V. Dispersion of nonresonant third-order nonlinearities in Silicon Carbide. *Sci. Rep.* **2017**, *7*, 40924.
(78) Cardenas, J.; Yu, M.; Okawachi, Y.; Poitras, C. B.; Lau, R. K. W.; Dutt, A.; Gaeta, A. L.; Lipson, M. Optical nonlinearities in high-confinement silicon carbide waveguides. *Opt. Lett.* **2015**, *40*, 4138−4141.
(79) Shi, X.; Fan, W.; Lu, Y.; Hansen, A. K.; Chi, M.; Yi, A.; Ou, X.; Rottwitt, K.; Ou, H. Polarization and spatial mode dependent four-wave mixing in a 4H-silicon carbide microring resonator. *APL Photonics* **2021**, *6*, 076106.
(80) Xing, P.; Ma, D.; Kimerling, L. C.; Agarwal, A. M.; Tan, D. T. High efficiency four wave mixing and optical bistability in amorphous silicon carbide ring resonators. *APL Photonics* **2020**, *5*, 076110.
(81) Wang, Y.; Lin, Q.; Feng, P. X.-L. Single-crystal 3C-SiC-on-insulator platform for integrated quantum photonics. *Opt. Express* **2021**, *29*, 1011−1022.
(82) Shi, X.; Fan, W.; Hansen, A. K.; Chi, M.; Yi, A.; Ou, X.; Rottwitt, K.; Ou, H. Thermal Behaviors and Optical Parametric Oscillation in 4H-Silicon Carbide Integrated Platforms. *Advanced Photonics Research* **2021**, *2*, 2100068.
(83) Fan, H.-T.; Xu, C.-H.; Wang, Z.-H.; Wang, G.; Liu, C.-J.; Liang, J.-K.; Chen, X.-L.; Wei, Z.-Y. Generation of broadband 17μJ mid-infrared femtosecond pulses at 3.75μm by silicon carbide crystal. *Opt. Lett.* **2014**, *39*, 6249−6252.
(84) Guidry, M. A.; Lukin, D. M.; Yang, K. Y.; Trivedi, R.; Vučković, J. Quantum optics of soliton microcombs. *Nat. Photonics* **2022**, *16*, 52−58.
(85) Shu, H.; Chang, L.; Lao, C.; Shen, B.; Xie, W.; Zhang, X.; Jin, M.; Tao, Y.; Chen, R.; Tao, Z.; Yu, S.; Yang, Q.-F.; Wang, X.; Bowers, J. E. Sub-milliwatt, widely-tunable coherent microcomb generation with feedback-free operation. *arXiv:2112.08904 (physics.optics)* **2021**, na.
(86) Šuminienė, A.; Jukna, V.; Šuminas, R.; Tamošauskas, G.; Dubietis, A. Femtosecond infrared supercontinuum generation in 6H-SiC crystal. *OSA Continuum* **2021**, *4*, 911−917.
(87) Naftaly, M.; Molloy, J.; Magnusson, B.; Andreev, Y.; Lanskii, G. Silicon carbide—a high-transparency nonlinear material for THz applications. *Opt. Express* **2016**, *24*, 2590−2595.
(88) Hillenbrand, R.; Taubner, T.; Keilmann, F. Phonon-enhanced light−matter interaction at the nanometre scale. *Nature* **2002**, *418*, 159−162.
(89) Schuller, J. A.; Zia, R.; Taubner, T.; Brongersma, M. L. Dielectric metamaterials based on electric and magnetic resonances of silicon carbide particles. *Phys. Rev. Lett.* **2007**, *99*, 107401.
(90) Caldwell, J. D.; Glembocki, O. J.; Francescato, Y.; Sharac, N.; Giannini, V.; Bezares, F. J.; Long, J. P.; Owrutsky, J. C.; Vurgaftman, I.; Tischler, J. G.; et al. Low-loss, extreme subdiffraction photon confinement via silicon carbide localized surface phonon polariton resonators. *Nano Lett.* **2013**, *13*, 3690−3697.
(91) Kiessling, R.; Tong, Y.; Giles, A. J.; Gewinner, S.; Schöllkopf, W.; Caldwell, J. D.; Wolf, M.; Paarmann, A. Surface Phonon Polariton Resonance Imaging Using Long-Wave Infrared-Visible Sum-Frequency Generation Microscopy. *ACS Photonics* **2019**, *6*, 3017−3023.
(92) Kim, J.; Dutta, A.; Naik, G. V.; Giles, A. J.; Bezares, F. J.; Ellis, C. T.; Tischler, J. G.; Mahmoud, A. M.; Caglayan, H.; Glembocki, O. J.; Kildishev, A. V.; Caldwell, J. D.; Boltasseva, A.; Engheta, N. Role of epsilon-near-zero substrates in the optical response of plasmonic antennas. *Optica* **2016**, *3*, 339−346.
(93) Ou, H.; Ou, Y.; Argyraki, A.; Schimmel, S.; Kaiser, M.; Wellmann, P.; Linnarsson, M. K.; Jokubavicius, V.; Sun, J.; Liljedahl, R.; Syvajarvi, M. Advances in wide bandgap SiC for optoelectronics. *Eur. Phys. J. B* **2014**, *87*, 58.
(94) Qian, X.; Jiang, P.; Yang, R. Anisotropic thermal conductivity of 4H and 6H silicon carbide measured using time-domain thermoreflectance. *Mater. Today Phys.* **2017**, *3*, 70−75.
(95) Wei, Y.; Ou, H. Photoluminescence Quantum Yield of Fluorescent Silicon Carbide Determined by an Integrating Sphere Setup. *ACS Omega* **2019**, *4*, 15488−15495.
(96) Wei, Y.; Tarekegne, A. T.; Ou, H. Double D-centers related donor-acceptor-pairs emission in fluorescent silicon carbide. *Opt. Mater. Express* **2019**, *9*, 295−303.
(97) Lebedev, A. A. Deep level centers in silicon carbide: A review. *Semiconductors* **1999**, *33*, 107−130.
(98) Round, H. J. A. Note on Carborundum. *Electr. World* **1907**, *49*, 308.
(99) Vlaskina, S. Silicon carbide LED. *Semiconductor Physics, Quantum Electronics and Optoelectronics* **2002**, *5*, 71−75.
(100) Zheludev, N. The life and times of the LED—a 100-year history. *Nat. Photonics* **2007**, *1*, 189−192.
(101) Fan, J.; Wu, X.; Chu, P. K. Low-dimensional SiC nanostructures: fabrication, luminescence, and electrical properties. *Prog. Mater. Sci.* **2006**, *51*, 983−1031.
(102) Wimbauer, T.; Meyer, B. K.; Hofstaetter, A.; Scharmann, A.; Overhof, H. Negatively charged Si vacancy in SiC: A comparison between theory and experiment. *Phys. Rev. B: Condens. Matter.* **1997**, *56*, 7384−7388.
(103) Son, N. T.; Hai, P. N.; Janzén, E. Carbon vacancy-related defect in 4H and 6H SiC. *Phys. Rev. B: Condens. Matter.* **2001**, *63*, 2012011−2012014.
(104) Mizuochi, N.; Yamasaki, S.; Takizawa, H.; Morishita, N.; Ohshima, T.; Itoh, H.; Isoya, J. Continuous-wave and pulsed EPR study of the negatively charged silicon vacancy with S = 3/2 and C3v symmetry in n-type 4H-SiC. *Phys. Rev. B Condens. Matter.* **2002**, *66*, 235202.
(105) Koehl, W. F.; Buckley, B. B.; Heremans, F. J.; Calusine, G.; Awschalom, D. D. Room temperature coherent control of defect spin qubits in silicon carbide. *Nature* **2011**, *479*, 84−87.
(106) Falk, A. L.; Buckley, B. B.; Calusine, G.; Koehl, W. F.; Dobrovitski, V. V.; Politi, A.; Zorman, C. A.; Feng, P. X.-L.; Awschalom, D. D. Polytype control of spin qubits in silicon carbide. *Nat. Commun.* **2013**, *4*, 1819.
(107) Christle, D. J.; Falk, A. L.; Andrich, P.; Klimov, P. V.; Hassan, J. U.; Son, N. T.; Janzén, E.; Ohshima, T.; Awschalom, D. D. Isolated electron spins in silicon carbide with millisecond coherence times. *Nat. Mater.* **2015**, *14*, 160−163.
(108) Klimov, P. V.; Falk, A. L.; Christle, D. J.; Dobrovitski, V. V.; Awschalom, D. D. Quantum entanglement at ambient conditions in a macroscopic solid-state spin ensemble. *Sci. Adv.* **2015**, *1*, No. e1501015.
(109) Zwier, O. V.; O'Shea, D.; Onur, A. R.; van der Wal, C. H. All-optical coherent population trapping with defect spin ensembles in silicon carbide. *Sci. Rep.* **2015**, *5*, 10931.
(110) Umeda, T.; Son, N. T.; Isoya, J.; Janzén, E.; Ohshima, T.; Morishita, N.; Itoh, H.; Gali, A.; Bockstedte, M. Identification of the

Carbon Antisite-Vacancy Pair in 4H-SiC. *Phys. Rev. Lett.* **2006**, *96*, 145501.
(111) Steeds, J. Photoluminescence study of the carbon antisite-vacancy pair in 4 H-and 6 H-SiC. *Phys. Rev. B Condens. Matter.* **2009**, *80*, 245202.
(112) Szász, K.; Ivády, V.; Abrikosov, I. A.; Janzén, E.; Bockstedte, M.; Gali, A. Spin and photophysics of carbon-antisite vacancy defect in 4 h silicon carbide: A potential quantum bit. *Phys. Rev. B Condens. Matter.* **2015**, *91*, 121201.
(113) Son, N. T.; Stenberg, P.; Jokubavicius, V.; Abe, H.; Ohshima, T.; Ul Hassan, J.; Ivanov, I. G. Energy levels and charge state control of the carbon antisite-vacancy defect in 4H-SiC. *Appl. Phys. Lett.* **2019**, *114*, 212105.
(114) von Bardeleben, H.; Rauls, E.; Gerstmann, U. Carbon vacancy-related centers in 3 C-silicon carbide: Negative-U properties and structural transformation. *Phys. Rev. B Condens. Matter.* **2020**, *101*, 184108.
(115) von Bardeleben, H. J.; Cantin, J. L.; Rauls, E.; Gerstmann, U. Identification and magneto-optical properties of the NV center in 4HSiC. *Phys. Rev. B Condens. Matter.* **2015**, *92*, 064104.
(116) von Bardeleben, H. J.; Cantin, J. L.; Csóré, A.; Gali, A.; Rauls, E.; Gerstmann, U. NV centers in 3C,4H, and 6H silicon carbide: A variable platform for solid-state qubits and nanosensors. *Phys. Rev. B Condens. Matter.* **2016**, *94*, 121202.
(117) Zargaleh, S. A.; von Bardeleben, H. J.; Cantin, J. L.; Gerstmann, U.; Hameau, S.; Eblé, B.; Gao, W. Electron paramagnetic resonance tagged high-resolution excitation spectroscopy of NV-centers in 4H-SiC. *Phys. Rev. B Condens. Matter.* **2018**, *98*, 214113.
(118) Mu, Z.; Zargaleh, S. A.; von Bardeleben, H. J.; Fröch, J. E.; Nonahal, M.; Cai, H.; Yang, X.; Yang, J.; Li, X.; Aharonovich, I.; Gao, W. Coherent Manipulation with Resonant Excitation and Single Emitter Creation of Nitrogen Vacancy Centers in 4H Silicon Carbide. *Nano Lett.* **2020**, *20*, 6142−6147.
(119) Wang, J.-F.; Yan, F.-F.; Li, Q.; Liu, Z.-H.; Liu, H.; Guo, G.-P.; Guo, L.-P.; Zhou, X.; Cui, J.-M.; Wang, J.; Zhou, Z.-Q.; Xu, X.-Y.; Xu, J.-S.; Li, C.-F.; Guo, G.-C. Coherent Control of Nitrogen-Vacancy Center Spins in Silicon Carbide at Room Temperature. *Phys. Rev. Lett.* **2020**, *124*, 223601.
(120) Tissot, B.; Burkard, G. Spin structure and resonant driving of spin-1/2 defects in SiC. *Phys. Rev. B Condens. Matter.* **2021**, *103*, 064106.
(121) Diler, B.; Whiteley, S. J.; Anderson, C. P.; Wolfowicz, G.; Wesson, M. E.; Bielejec, E. S.; Joseph Heremans, F.; Awschalom, D. D. Coherent control and high-fidelity readout of chromium ions in commercial silicon carbide. *Npj Quantum Inf* **2020**, *6*, 1−6.
(122) Bosma, T.; Lof, G. J. J.; Gilardoni, C. M.; Zwier, O. V.; Hendriks, F.; Magnusson, B.; Ellison, A.; Gällström, A.; Ivanov, I. G.; Son, N. T.; Havenith, R. W. A.; van der Wal, C. H. Identification and tunable optical coherent control of transition-metal spins in silicon carbide. *Npj Quantum Inf* **2018**, *4*, 1−7.
(123) Gilardoni, C. M.; Bosma, T.; van Hien, D.; Hendriks, F.; Magnusson, B.; Ellison, A.; Ivanov, I. G.; Son, N. T.; van der Wal, C. H. Spin-relaxation times exceeding seconds for color centers with strong spin−orbit coupling in SiC. *New J. Phys.* **2020**, *22*, 103051.
(124) Wolfowicz, G.; Anderson, C. P.; Diler, B.; Poluektov, O. G.; Heremans, F. J.; Awschalom, D. D. Vanadium spin qubits as telecom quantum emitters in silicon carbide. *Sci. Adv.* **2020**, *6*, No. eaaz1192.
(125) Spindlberger, L.; Csóré, A.; Thiering, G.; Putz, S.; Karhu, R.; Hassan, J.; Son, N.; Fromherz, T.; Gali, A.; Trupke, M. Optical Properties of Vanadium in 4H Silicon Carbide for Quantum Technology. *Phys. Rev. Applied* **2019**, *12*, 014015.
(126) Yan, F.-F.; Yi, A.-L.; Wang, J.-F.; Li, Q.; Yu, P.; Zhang, J.-X.; Gali, A.; Wang, Y.; Xu, J.-S.; Ou, X.; Li, C.-F.; Guo, G.-C. Room-temperature coherent control of implanted defect spins in silicon carbide. *Npj Quantum Inf* **2020**, *6*, 1−6.
(127) Koehl, W. F.; Buckley, B. B.; Heremans, F. J.; Calusine, G.; Awschalom, D. D. Room temperature coherent control of defect spin qubits in silicon carbide. *Nature* **2011**, *479*, 84.
(128) Castelletto, S.; Boretti, A. Silicon carbide color centers for quantum applications. *JPhys. Photonics* **2020**, *2*, 022001.
(129) Sörman, E.; Son, N. T.; Chen, W. M.; Kordina, O.; Hallin, C.; Janzén, E. Silicon vacancy related defect in 4H and 6H SiC. *Phys. Rev. B Condens. Matter.* **2000**, *61*, 2613−2620.
(130) Janzén, E.; Gali, A.; Carlsson, P.; Gällström, A.; Magnusson, B.; Son, N. T. The silicon vacancy in SiC. *Phys. B: Condens. Matter* **2009**, *404*, 4354−4358.
(131) Baranov, P. G.; Bundakova, A. P.; Soltamova, A. A.; Orlinskii, S. B.; Borovykh, I. V.; Zondervan, R.; Verberk, R.; Schmidt, J. Silicon vacancy in SiC as a promising quantum system for single-defect and single-photon spectroscopy. *Phys. Rev. B: Condens. Matter.* **2011**, *83*, 1−12.
(132) Soltamov, V. A.; Soltamova, A. A.; Baranov, P. G.; Proskuryakov, I. I. Room temperature coherent spin alignment of silicon vacancies in 4H- and 6H-SiC. *Phys. Rev. Lett.* **2012**, *108*, 4−7.
(133) Hain, T. C.; Fuchs, F.; Soltamov, V. A.; Baranov, P. G.; Astakhov, G. V.; Hertel, T.; Dyakonov, V. Excitation and recombination dynamics of vacancy-related spin centers in silicon carbide. *J. Appl. Phys.* **2014**, *115*, 133508.
(134) Fuchs, F.; Stender, B.; Trupke, M.; Simin, D.; Pflaum, J.; Dyakonov, V.; Astakhov, G. V. Engineering near-infrared single-photon emitters with optically active spins in ultrapure silicon carbide. *Nat. Commun.* **2015**, *6*, 1−7.
(135) Carter, S. G.; Soykal, Ö. O.; Dev, P.; Economou, S. E.; Glaser, E. R. Spin coherence and echo modulation of the silicon vacancy in 4H-SiC at room temperature. *Phys. Rev. B: Condens. Matter.* **2015**, *92*, No. 161202.
(136) Soltamov, V. A.; Yavkin, B. V.; Tolmachev, D. O.; Babunts, R. A.; Badalyan, A. G.; Davydov, V. Y.; Mokhov, E. N.; Proskuryakov, I. I.; Orlinskii, S. B.; Baranov, P. G. Optically Addressable Silicon Vacancy-Related Spin Centers in Rhombic Silicon Carbide with High Breakdown Characteristics and ENDOR Evidence of Their Structure. *Phys. Rev. Lett.* **2015**, *115*, 247602.
(137) Economou, S. E.; Dev, P. Spin-photon entanglement interfaces in silicon carbide defect centers. *Nanotechnology* **2016**, *27*, 504001.
(138) Soykal, Ö. O.; Dev, P.; Economou, S. E. Silicon vacancy center in 4H-SiC: Electronic structure and spin-photon interfaces. *Phys. Rev. B Condens. Matter.* **2016**, *93*, 081207.
(139) Ivády, V.; Davidsson, J.; Tien Son, N.; Ohshima, T.; Abrikosov, I.; Gali, A. Identification of Si-vacancy related room temperature qubits in 4H silicon carbide. *Phys. Rev. B: Condens. Matter.* **2017**, *96*, No. 161114.
(140) Bracher, D. O.; Zhang, X.; Hu, E. L. Selective Purcell enhancement of two closely linked zero-phonon transitions of a silicon carbide color center. *Proc. Natl. Acad. Sci. U. S. A.* **2017**, *114*, 4060−4065.
(141) Nagy, R.; Widmann, M.; Niethammer, M.; Dasari, D. B.; Gerhardt, I.; Soykal, Ö. O.; Radulaski, M.; Ohshima, T.; Vučković, J.; Son, N. T.; Ivanov, I. G.; Economou, S. E.; Bonato, C.; Lee, S. Y.; Wrachtrup, J. Quantum Properties of Dichroic Silicon Vacancies in Silicon Carbide. *Phys. Rev. Applied* **2018**, *9*, 034022.
(142) Fischer, M.; Sperlich, A.; Kraus, H.; Ohshima, T.; Astakhov, G. V.; Dyakonov, V. Highly Efficient Optical Pumping of Spin Defects in Silicon Carbide for Stimulated Microwave Emission. *Phys. Rev. Appl.* **2018**, *9*, 54006.
(143) Tarasenko, S. A.; Poshakinskiy, A. V.; Simin, D.; Soltamov, V. A.; Mokhov, E. N.; Baranov, P. G.; Dyakonov, V.; Astakhov, G. V. Spin and Optical Properties of Silicon Vacancies in Silicon Carbide: A Review. *Phys. Status Solidi B: Basic Res.* **2018**, *255*, 1700258.
(144) Davidsson, J.; Ivády, V.; Armiento, R.; Ohshima, T.; Son, N. T.; Gali, A.; Abrikosov, I. A. Identification of divacancy and silicon vacancy qubits in 6H-SiC. *Appl. Phys. Lett.* **2019**, *114*, 112107.
(145) Banks, H. B.; Soykal, Ö. O.; Myers-Ward, R. L.; Gaskill, D. K.; Reinecke, T. L.; Carter, S. G. Resonant Optical Spin Initialization and Readout of Single Silicon Vacancies in 4H - Si C. *Phys. Rev. Applied* **2019**, *11*, 1.

https://doi.org/10.1021/acsphotonics.1c01775
ACS Photonics 2022, 9, 1434−1457

(146) Udvarhelyi, P.; Nagy, R.; Kaiser, F.; Lee, S. Y.; Wrachtrup, J.; Gali, A. Spectrally Stable Defect Qubits with no Inversion Symmetry for Robust Spin-To-Photon Interface. *Phys. Rev. Appl.* **2019**, *11*, 1.
(147) Dong, W.; Doherty, M. W.; Economou, S. E. Spin polarization through intersystem crossing in the silicon vacancy of silicon carbide. *Phys. Rev. B Condens. Matter.* **2019**, *99*, 184102.
(148) Bathen, M. E.; Galeckas, A.; Müting, J.; Ayedh, H. M.; Grossner, U.; Coutinho, J.; Frodason, Y. K.; Vines, L. Electrical charge state identification and control for the silicon vacancy in 4H-SiC. *npj Quantum Inf* **2019**, *5*, 111.
(149) Shang, Z.; Hashemi, A.; Berencén, Y.; Komsa, H. P.; Erhart, P.; Zhou, S.; Helm, M.; Krasheninnikov, A. V.; Astakhov, G. V. Local vibrational modes of Si vacancy spin qubits in SiC. *Phys. Rev. B Condens. Matter.* **2020**, *101*, 1−9.
(150) Rühl, M.; Bergmann, L.; Krieger, M.; Weber, H. B. Stark Tuning of the Silicon Vacancy in Silicon Carbide. *Nano Lett.* **2020**, *20*, 658−663.
(151) Vásquez, G. C.; Bathen, M. E.; Galeckas, A.; Bazioti, C.; Johansen, K. M.; Maestre, D.; Cremades, A.; Prytz; Moe, A. M.; Kuznetsov, A. Y.; Vines, L. Strain Modulation of Si Vacancy Emission from SiC Micro- And Nanoparticles. *Nano Lett.* **2020**, *20*, 8689−8695.
(152) Singh, H.; Anisimov, A. N.; Nagalyuk, S. S.; Mokhov, E. N.; Baranov, P. G.; Suter, D. Experimental characterization of spin-3/2 silicon vacancy centers in 6H-SiC. *Phys. Rev. B Condens. Matter.* **2020**, *101*, 134110.
(153) Nagy, R.; et al. Narrow inhomogeneous distribution of spin-active emitters in silicon carbide. *Appl. Phys. Lett.* **2021**, *118*, 144003.
(154) Shang, Z.; Berencén, Y.; Hollenbach, M.; Zhou, S.; Kraus, H.; Ohshima, T.; Astakhov, G. Microwave-Assisted Spectroscopy of Vacancy-Related Spin Centers in Hexagonal SiC. *Phys. Rev. Applied* **2021**, *15*, 034059.
(155) Breev, I. D.; Shang, Z.; Poshakinskiy, A. V.; Singh, H.; Berencén, Y.; Hollenbach, M.; Nagalyuk, S. S.; Mokhov, E. N.; Babunts, R. A.; Baranov, P. G.; Suter, D.; Tarasenko, S. A.; Astakhov, G. V.; Anisimov, A. N. Inverted fine structure of a 6H-SiC qubit enabling robust spin-photon interface. *Npj Quantum Inf* **2022**, *8*, 1−9.
(156) Anisimov, A. N.; Nagalyuk, S. S.; Muzafarova, M. V.; Bundakova, A. P.; Babunts, R. A.; Soltamov, V. A.; Mokhov, E. N.; Baranov, P. G. Spin Diagnostics of Local Polytypic Composition of Silicon Carbide with Submicron Spatial Resolution. *Appl. Magn. Reson.* **2019**, *50*, 323−331.
(157) Christle, D. J.; Klimov, P. V.; de las Casas, C. F.; Szász, K.; Ivády, V.; Jokubavicius, V.; Ul Hassan, J.; Syväjärvi, M.; Koehl, W. F.; Ohshima, T.; Son, N. T.; Janzén, E.; Gali, d.; Awschalom, D. D. Isolated Spin Qubits in SiC with a High-Fidelity Infrared Spin-to-Photon Interface. *Phys. Rev. X* **2017**, *7*, 021046.
(158) Miao, K. C.; Blanton, J. P.; Anderson, C. P.; Bourassa, A.; Crook, A. L.; Wolfowicz, G.; Abe, H.; Ohshima, T.; Awschalom, D. D. Universal coherence protection in a solid-state spin qubit. *Science* **2020**, *369*, 1493−1497.
(159) Onizhuk, M.; Miao, K. C.; Blanton, J. P.; Ma, H.; Anderson, C. P.; Bourassa, A.; Awschalom, D. D.; Galli, G. Probing the Coherence of Solid-State Qubits at Avoided Crossings. *PRX Quantum* **2021**, *2*, 010311.
(160) Jurgen von Bardeleben, H.; Cantin, J.-L.; Gerstmann, U.; Schmidt, W. G.; Biktagirov, T. Spin Polarization, Electron−Phonon Coupling, and Zero-Phonon Line of the NV Center in 3 C-SiC. *Nano Lett.* **2021**, *21*, 8119−8125.
(161) Tissot, B.; Burkard, G. Hyperfine structure of transition metal defects in SiC. *Phys. Rev. B Condens. Matter.* **2021**, *104*, 064102.
(162) Di Cioccio, L.; Le Tiec, Y.; Letertre, F.; Jaussaud, C.; Bruel, M. Silicon carbide on insulator formation using the Smart Cut process. *Electron. Lett.* **1996**, *32*, 1144−1145.
(163) Martini, F.; Politi, A. Linear integrated optics in 3C silicon carbide. *Opt. Express* **2017**, *25*, 10735−10742.
(164) Shishkin, Y.; Choyke, W. J.; Devaty, R. P. Photoelectrochemical etching of n-type 4H silicon carbide. *J. Appl. Phys.* **2004**, *96*, 2311−2322.
(165) Lukin, D. M.; Guidry, M. A.; Vučković, J. Integrated Quantum Photonics with Silicon Carbide: Challenges and Prospects. *PRX Quantum* **2020**, *1*, 020102.
(166) Di Cioccio, L.; Letertre, F.; Le Tiec, Y.; Papon, A.; Jaussaud, C.; Bruel, M. Silicon carbide on insulator formation by the Smart-Cut process. *Mater. Sci. Eng. B: Solid-State Mater. Adv. Technol.* **1997**, *46*, 349−356.
(167) Song, B.-S.; Yamada, S.; Asano, T.; Noda, S. Demonstration of two-dimensional photonic crystals based on silicon carbide. *Opt. Express* **2011**, *19*, 11084−11089.
(168) Fan, T.; Wu, X.; Eftekhar, A. A.; Bosi, M.; Moradinejad, H.; Woods, E. V.; Adibi, A. High-quality integrated microdisk resonators in the visible-to-near-infrared wavelength range on a 3C-silicon carbide-on-insulator platform. *Opt. Lett.* **2020**, *45*, 153−156.
(169) Song, B.-S.; Jeon, S.; Kim, H.; Kang, D. D.; Asano, T.; Noda, S. High-Q-factor nanobeam photonic crystal cavities in bulk silicon carbide. *Appl. Phys. Lett.* **2018**, *113*, 231106.
(170) Garrisi, F.; Chatzopoulos, I.; Cernansky, R.; Politi, A. Silicon carbide photonic platform based on suspended subwavelength waveguides. *J. Opt. Soc. Am. B* **2020**, *37*, 3453−3460.
(171) Tang, X.; Wongchotigul, K.; Spencer, M. G. Optical waveguide formed by cubic silicon carbide on sapphire substrates. *Appl. Phys. Lett.* **1991**, *58*, 917−918.
(172) Powell, K.; Shams-Ansari, A.; Desai, S.; Austin, M.; Deng, J.; Sinclair, N.; Lončar, M.; Yi, X. High-Q suspended optical resonators in 3C silicon carbide obtained by thermal annealing. *Opt. Express* **2020**, *28*, 4938−4949.
(173) Yamada, S.; Song, B.-S.; Asano, T.; Noda, S. Silicon carbide-based photonic crystal nanocavities for ultra-broadband operation from infrared to visible wavelengths. *Appl. Phys. Lett.* **2011**, *99*, 201102.
(174) Yamada, S.; Song, B.-S.; Jeon, S.; Upham, J.; Tanaka, Y.; Asano, T.; Noda, S. Second-harmonic generation in a silicon-carbide-based photonic crystal nanocavity. *Opt. Lett.* **2014**, *39*, 1768−1771.
(175) Radulaski, M.; Babinec, T. M.; Buckley, S.; Rundquist, A.; Provine, J.; Alassaad, K.; Ferro, G.; Vučković, J. Photonic crystal cavities in cubic (3C) polytype silicon carbide films. *Opt. Express* **2013**, *21*, 32623−32629.
(176) Calusine, G.; Politi, A.; Awschalom, D. D. Silicon carbide photonic crystal cavities with integrated color centers. *Appl. Phys. Lett.* **2014**, *105*, 011123.
(177) Lee, J. Y.; Lu, X.; Lin, Q. High-Q silicon carbide photonic-crystal cavities. *Appl. Phys. Lett.* **2015**, *106*, 041106.
(178) Calusine, G.; Politi, A.; Awschalom, D. D. Cavity-Enhanced Measurements of Defect Spins in Silicon Carbide. *Phys. Rev. Applied* **2016**, *6*, 014019.
(179) Bracher, D. O.; Hu, E. L. Fabrication of high-Q nanobeam photonic crystals in epitaxially grown 4H-SiC. *Nano Lett.* **2015**, *15*, 6202−6207.
(180) Crook, A. L.; Anderson, C. P.; Miao, K. C.; Bourassa, A.; Lee, H.; Bayliss, S. L.; Bracher, D. O.; Zhang, X.; Abe, H.; Ohshima, T.; et al. Purcell enhancement of a single silicon carbide color center with coherent spin control. *Nano Lett.* **2020**, *20*, 3427−3434.
(181) Xing, P.; Ma, D.; Kimerling, L. C.; Agarwal, A. M.; Tan, D. T. H. High efficiency four wave mixing and optical bistability in amorphous silicon carbide ring resonators. *APL Photonics* **2020**, *5*, 076110.
(182) Fan, T.; Wu, X.; Vangapandu, S. R. M.; Hosseinnia, A. H.; Eftekhar, A. A.; Adibi, A. Racetrack microresonator based electro-optic phase shifters on a 3C silicon-carbide-on-insulator platform. *Opt. Lett.* **2021**, *46*, 2135−2138.
(183) Powell, K.; Li, L.; Shams-Ansari, A.; Wang, J.; Meng, D.; Sinclair, N.; Deng, J.; Lončar, M.; Yi, X. Integrated silicon carbide modulator for CMOS photonics. https://www.researchsquare.com/article/rs-178354/v1, Submission Date 02/05/2021, Preprint Research Square, Accessed: 2022−03−08.
(184) Cranwell Schaeper, O.; Fröch, J. E.; Kim, S.; Mu, Z.; Toth, M.; Gao, W.; Aharonovich, I. Fabrication of Photonic Resonators in Bulk 4H-SiC. *Adv. Mater. Technol.* **2021**, *6*, 2100589.

(185) Cardenas, J.; Zhang, M.; Phare, C. T.; Shah, S. Y.; Poitras, C. B.; Guha, B.; Lipson, M. High q sic microresonators. *Opt. Express* **2013**, *21*, 16882−16887.
(186) Lu, X.; Lee, J. Y.; Feng, P. X.-L.; Lin, Q. Silicon carbide microdisk resonator. *Opt. Lett.* **2013**, *38*, 1304−1306.
(187) Magyar, A. P.; Bracher, D.; Lee, J. C.; Aharonovich, I.; Hu, E. L. High quality SiC microdisk resonators fabricated from monolithic epilayer wafers. *Appl. Phys. Lett.* **2014**, *104*, 051109.
(188) Radulaski, M.; Babinec, T. M.; Müller, K.; Lagoudakis, K. G.; Zhang, J. L.; Buckley, S.; Kelaita, Y. A.; Alassaad, K.; Ferro, G.; Vučković, J. Visible photoluminescence from cubic (3C) silicon carbide microdisks coupled to high quality whispering gallery modes. *ACS Photonics* **2015**, *2*, 14−19.
(189) Lohrmann, A.; Karle, T. J.; Sewani, V. K.; Laucht, A.; Bosi, M.; Negri, M.; Castelletto, S.; Prawer, S.; McCallum, J. C.; Johnson, B. C. Integration of single-photon emitters into 3C-SiC microdisk resonators. *ACS Photonics* **2017**, *4*, 462−468.
(190) Radulaski, M.; Zhang, J. L.; Tzeng, Y.-K.; Lagoudakis, K. G.; Ishiwata, H.; Dory, C.; Fischer, K. A.; Kelaita, Y. A.; Sun, S.; Maurer, P. C.; et al. Nanodiamond integration with photonic devices. *Laser Photonics Rev.* **2019**, *13*, 1800316.
(191) Wang, C.; Shen, C.; Yi, A.; Yang, S.; Zhou, L.; Zhu, Y.; Huang, K.; Song, S.; Zhou, M.; Zhang, J.; Ou, X. Visible and near-infrared microdisk resonators on a 4H-silicon-carbide-on-insulator platform. *Opt. Lett.* **2021**, *46*, 2952−2955.
(192) Jia, H.; Wu, X.; Tang, H.; Lu, Z.-R.; Feng, P. X.-L. Culturing and probing physical behavior of individual breast cancer cells on SiC microdisk resonators. *28th IEEE International Conference on Micro Electro Mechanical Systems (MEMS)*, Estoril, Portugal, January 18−22, 2015, IEEE, 2015; pp 698−701.
(193) Yang, R.; Wang, Z.; Lee, J.; Ladhane, K.; Young, D. J.; Feng, P. X.-L. 6H-SiC microdisk torsional resonators in a "smart-cut" technology. *Appl. Phys. Lett.* **2014**, *104*, 091906.
(194) Wang, Z.; Lee, J.; Feng, P. X.-L. Spatial mapping of multimode Brownian motions in high-frequency silicon carbide microdisk resonators. *Nat. Commun.* **2014**, *5*, 1−11.
(195) Lu, X.; Lee, J. Y.; Lin, Q. High-frequency and high-quality silicon carbide optomechanical microresonators. *Sci. Rep.* **2015**, *5*, 1−9.
(196) Lu, X.; Lee, J. Y.; Lin, Q. Silicon carbide zipper photonic crystal optomechanical cavities. *Appl. Phys. Lett.* **2020**, *116*, 221104.
(197) Lu, X.; Lee, J. Y.; Rogers, S. D.; Lin, Q. Silicon carbide double-microdisk resonator. *Opt. Lett.* **2019**, *44*, 4295−4298.
(198) Tiecke, T. G.; Nayak, K. P.; Thompson, J. D.; Peyronel, T.; de Leon, N. P.; Vuletić, V.; Lukin, M. D. Efficient fiber-optical interface for nanophotonic devices. *Optica* **2015**, *2*, 70−75.
(199) Burek, M. J.; Meuwly, C.; Evans, R. E.; Bhaskar, M. K.; Sipahigil, A.; Meesala, S.; Machielse, B.; Sukachev, D. D.; Nguyen, C. T.; Pacheco, J. L.; Bielejec, E.; Lukin, M. D.; Lončar, M. Fiber-Coupled Diamond Quantum Nanophotonic Interface. *Phys. Rev. Applied* **2017**, *8*, 024026.
(200) Castelletto, S.; Johnson, B. C.; Zachreson, C.; Beke, D.; Balogh, I.; Ohshima, T.; Aharonovich, I.; Gali, A. Room Temperature Quantum Emission from Cubic Silicon Carbide Nanoparticles. *ACS Nano* **2014**, *8*, 7938−7947.
(201) Castelletto, S.; Bodrog, Z.; Magyar, A. P.; Gentle, A.; Gali, A.; Aharonovich, I. Quantum-confined single photon emission at room temperature from SiC tetrapods. *Nanoscale* **2014**, *6*, 10027−10032.
(202) Lienhard, B.; Schröder, T.; Mouradian, S.; Dolde, F.; Tran, T. T.; Aharonovich, I.; Englund, D. Bright and photostable single-photon emitter in silicon carbide. *Optica* **2016**, *3*, 768−774.
(203) Lohrmann, A.; Castelletto, S.; Klein, J. R.; Ohshima, T.; Bosi, M.; Negri, M.; Lau, D. W. M.; Gibson, B. C.; Prawer, S.; McCallum, J. C.; Johnson, B. C. Activation and control of visible single defects in 4H-, 6H-, and 3C-SiC by oxidation. *Appl. Phys. Lett.* **2016**, *108*, 021107.
(204) Abe, Y.; Umeda, T.; Okamoto, M.; Kosugi, R.; Harada, S.; Haruyama, M.; Kada, W.; Hanaizumi, O.; Onoda, S.; Ohshima, T. Single photon sources in 4H-SiC metal-oxide-semiconductor field-effect transistors. *Appl. Phys. Lett.* **2018**, *112*, 031105.
(205) Johnson, B.; Woerle, J.; Haasmann, D.; Lew, C.-K.; Parker, R.; Knowles, H.; Pingault, B.; Atature, M.; Gali, A.; Dimitrijev, S.; Camarda, M.; McCallum, J. Optically Active Defects at the SiC/SiO_2 Interface. *Phys. Rev. Applied* **2019**, *12*, 044024.
(206) Wang, J.; Zhou, Y.; Wang, Z.; Rasmita, A.; Yang, J.; Li, X.; von Bardeleben, H. J.; Gao, W. Bright room temperature single photon source at telecom range in cubic silicon carbide. *Nat. Commun.* **2018**, *9*, 4106.
(207) Pavunny, S. P.; Yeats, A. L.; Banks, H. B.; Bielejec, E.; Myers-Ward, R. L.; DeJarld, M. T.; Bracker, A. S.; Gaskill, D. K.; Carter, S. G. Arrays of Si vacancies in 4H-SiC produced by focused Li ion beam implantation. *Sci. Rep.* **2021**, *11*, 1−8.
(208) Chen, Y.-C.; Salter, P. S.; Niethammer, M.; Widmann, M.; Kaiser, F.; Nagy, R.; Morioka, N.; Babin, C.; Erlekampf, J.; Berwian, P.; et al. Laser writing of scalable single color centers in silicon carbide. *Nano Lett.* **2019**, *19*, 2377−2383.
(209) Castelletto, S.; Maksimovic, J.; Katkus, T.; Ohshima, T.; Johnson, B. C.; Juodkazis, S. Color centers enabled by direct femtosecond laser writing in wide bandgap semiconductors. *Nanomaterials* **2021**, *11*, 72.
(210) Lohrmann, A.; Iwamoto, N.; Bodrog, Z.; Castelletto, S.; Ohshima, T.; Karle, T.; Gali, A.; Prawer, S.; McCallum, J.; Johnson, B. Single-photon emitting diode in silicon carbide. *Nat. Commun.* **2015**, *6*, 1−7.
(211) Sato, S.-i.; Honda, T.; Makino, T.; Hijikata, Y.; Lee, S.-Y.; Ohshima, T. Room temperature electrical control of single photon sources at 4H-SiC surface. *ACS Photonics* **2018**, *5*, 3159−3165.
(212) Widmann, M.; Niethammer, M.; Makino, T.; Rendler, T.; Lasse, S.; Ohshima, T.; Ul Hassan, J.; Tien Son, N.; Lee, S.-Y.; Wrachtrup, J. Bright single photon sources in lateral silicon carbide light emitting diodes. *Appl. Phys. Lett.* **2018**, *112*, 231103.
(213) Castelletto, S.; Al Atem, A. S.; Inam, F. A.; von Bardeleben, H. J.; Hameau, S.; Almutairi, A. F.; Guillot, G.; Sato, S.-i.; Boretti, A.; Bluet, J. M. Deterministic placement of ultra-bright near-infrared color centers in arrays of silicon carbide micropillars. *Beilstein J. Nanotechnol.* **2019**, *10*, 2383−2395.
(214) Parker, R. A.; Dontschuk, N.; Sato, S.-I.; Lew, C. T.-K.; Reineck, P.; Nadarajah, A.; Ohshima, T.; Gibson, B. C.; Castelletto, S.; McCallum, J. C.; Johnson, B. C. Infrared erbium photoluminescence enhancement in silicon carbide nano-pillars. *J. Appl. Phys.* **2021**, *130*, 145101.
(215) Inam, F. A.; Castelletto, S. Understanding the photonics of single color-center emission in a high-indexed nano-pillar. *J. Appl. Phys.* **2021**, *130*, 083102.
(216) Inam, F. A.; Castelletto, S. Using multi-polar scattering and near-field plasmonic resonances to achieve optimal emission enhancement from quantum emitters embedded in dielectric pillars. *J. Opt. Soc. Am. B* **2021**, *38*, 3697−3704.
(217) Torun, C. G.; Schneider, P.-I.; Hammerschmidt, M.; Burger, S.; Munns, J. H. D.; Schröder, T. Optimized diamond inverted nanocones for enhanced color center to fiber coupling. *Appl. Phys. Lett.* **2021**, *118*, 234002.
(218) Pfender, M.; et al. Protecting a Diamond Quantum Memory by Charge State Control. *Nano Lett.* **2017**, *17*, 5931−5937.
(219) Hefner, A.; Singh, R.; Lai, J.-S.; Berning, D.; Bouche, S.; Chapuy, C. SiC power diodes provide breakthrough performance for a wide range of applications. *IEEE Trans. Power Electron* **2001**, *16*, 273−280.
(220) Rozpedek, F.; Yehia, R.; Goodenough, K.; Ruf, M.; Humphreys, P. C.; Hanson, R.; Wehner, S.; Elkouss, D. Near-term quantum-repeater experiments with nitrogen-vacancy centers: Overcoming the limitations of direct transmission. *Phys. Rev. A* **2019**, *99*, 052330.
(221) Preskill, J. Quantum Computing in the NISQ era and beyond. *Quantum* **2018**, *2*, 79.
(222) Brooks, M. Beyond quantum supremacy: the hunt for useful quantum computers. *Nature* **2019**, *574*, 19−21.
(223) Wolfowicz, G.; Heremans, F. J.; Anderson, C. P.; Kanai, S.; Seo, H.; Gali, A.; Galli, G.; Awschalom, D. D. Quantum guidelines for solid-state spin defects. *Nat. Rev. Mater.* **2021**, *6*, 906.
(224) Weber, J. H.; Kambs, B.; Kettler, J.; Kern, S.; Maisch, J.; Vural, H.; Jetter, M.; Portalupi, S. L.; Becher, C.; Michler, P. Two-photon

interference in the telecom C-band after frequency conversion of photons from remote quantum emitters. *Nat. Nanotechnol.* **2019**, *14*, 23−26.
(225) Whiteley, S. J.; Wolfowicz, G.; Anderson, C. P.; Bourassa, A.; Ma, H.; Ye, M.; Koolstra, G.; Satzinger, K. J.; Holt, M. V.; Heremans, F. J.; et al. Spin−phonon interactions in silicon carbide addressed by Gaussian acoustics. *Nat. Phys.* **2019**, *15*, 490−495.
(226) Bourassa, A.; Anderson, C. P.; Miao, K. C.; Onizhuk, M.; Ma, H.; Crook, A. L.; Abe, H.; Ul-Hassan, J.; Ohshima, T.; Son, N. T.; et al. Entanglement and control of single nuclear spins in isotopically engineered silicon carbide. *Nat. Mater.* **2020**, *19*, 1319−1325.
(227) Ruhl, M.; Bergmann, L.; Krieger, M.; Weber, H. B. Stark tuning of the silicon vacancy in silicon carbide. *Nano Lett.* **2020**, *20*, 658−663.
(228) Gschrey, M.; Thoma, A.; Schnauber, P.; Seifried, M.; Schmidt, R.; Wohlfeil, B.; Krüger, L.; Schulze, J. H.; Heindel, T.; Burger, S.; Schmidt, F.; Strittmatter, A.; Rodt, S.; Reitzenstein, S. Highly indistinguishable photons from deterministic quantum-dot microlenses utilizing three-dimensional in situ electron-beam lithography. *Nat. Commun.* **2015**, *6*, 1−8.
(229) Thoma, A.; Schnauber, P.; Gschrey, M.; Seifried, M.; Wolters, J.; Schulze, J. H.; Strittmatter, A.; Rodt, S.; Carmele, A.; Knorr, A.; Heindel, T.; Reitzenstein, S. Exploring Dephasing of a Solid-State Quantum Emitter via Time- and Temperature-Dependent Hong-Ou-Mandel Experiments. *Phys. Rev. Lett.* **2016**, *116*, 033601.
(230) Bernien, H.; Childress, L.; Robledo, L.; Markham, M.; Twitchen, D.; Hanson, R. Two-Photon Quantum Interference from Separate Nitrogen Vacancy Centers in Diamond. *Phys. Rev. Lett.* **2012**, *108*, 043604.
(231) Rezai, M.; Wrachtrup, J.; Gerhardt, I. Polarization-entangled photon pairs from a single molecule. *Optica* **2019**, *6*, 34.
(232) Lindner, N. H.; Rudolph, T. Proposal for Pulsed On-Demand Sources of Photonic Cluster State Strings. *Phys. Rev. Lett.* **2009**, *103*, 113602.
(233) Raha, M.; Chen, S.; Phenicie, C. M.; Ourari, S.; Dibos, A. M.; Thompson, J. D. Optical quantum nondemolition measurement of a single rare earth ion qubit. *Nat. Commun.* **2020**, *11*, 1605.
(234) Economou, S. E.; Dev, P. Spin-photon entanglement interfaces in silicon carbide defect centers. *Nanotechnology* **2016**, *27*, 504001.
(235) Castelletto, S.; Johnson, B.; Boretti, A. Quantum effects in silicon carbide hold promise for novel integrated devices and sensors. *Adv. Opt. Mater.* **2013**, *1*, 609−625.
(236) Ivády, V.; Davidsson, J.; Delegan, N.; Falk, A. L.; Klimov, P. V.; Whiteley, S. J.; Hruszkewycz, S. O.; Holt, M. V.; Heremans, F. J.; Son, N. T.; Awschalom, D. D.; Abrikosov, I. A.; Gali, A. Stabilization of point-defect spin qubits by quantum wells. *Nat. Commun.* **2019**, *10*, 5607.
(237) McCloskey, D. J.; Dontschuk, N.; Broadway, D. A.; Nadarajah, A.; Stacey, A.; Tetienne, J.-P.; Hollenberg, L. C.; Prawer, S.; Simpson, D. A. Enhanced widefield quantum sensing with nitrogen-vacancy ensembles using diamond nanopillar arrays. *ACS Appl. Mater. Interfaces* **2020**, *12*, 13421−13427.
(238) Schrinner, P. P.; Olthaus, J.; Reiter, D. E.; Schuck, C. Integration of Diamond-Based Quantum Emitters with Nanophotonic Circuits. *Nano Lett.* **2020**, *20*, 8170−8177.
(239) Jung, T.; Görlitz, J.; Kambs, B.; Pauly, C.; Raatz, N.; Nelz, R.; Neu, E.; Edmonds, A. M.; Markham, M.; Mücklich, F.; Meijer, J.; Becher, C. Spin measurements of NV centers coupled to a photonic crystal cavity. *APL Photonics* **2019**, *4*, 120803.
(240) Lin, W.-X.; Yan, F.-F.; Li, Q.; Wang, J.-f.; Hao, Z.-H.; Zhou, J.-Y.; Li, H.; You, L.-X.; Xu, J.-S.; Li, C.-F.; Guo, G.-C. Temperature dependence of divacancy spin coherence in implanted silicon carbide. *Phys. Rev. B Condens. Matter.* **2021**, *104*, 125305.
(241) Latka, I.; Ecke, W.; Höfer, B.; Chojetzki, C.; Reutlinger, A. Fiber optic sensors for the monitoring of cryogenic spacecraft tank structures. *Photonics North 2004: Photonic Applications in Telecommunications, Sensors, Software, and Lasers*; SPIE, 2004; pp 195−204.
(242) Saddow, S. E. *Silicon Carbide Biotechnology: A Biocompatible Semiconductor for Advanced Biomedical Devices and Applications*; Elsevier, 2012.
(243) Hruszkewycz, S. O.; Maddali, S.; Anderson, C. P.; Cha, W.; Miao, K. C.; Highland, M. J.; Ulvestad, A.; Awschalom, D. D.; Heremans, F. J. Strain annealing of SiC nanoparticles revealed through Bragg coherent diffraction imaging for quantum technologies. *Phys. Rev. Materials* **2018**, *2*, 086001.
(244) Beke, D.; Valenta, J.; Karolyhazy, G.; Lenk, S.; Czigany, Z.; Markus, B. G.; Kamaras, K.; Simon, F.; Gali, A. Room-temperature defect qubits in ultrasmall nanocrystals. *J. Phys. Chem. Lett.* **2020**, *11*, 1675−1681.
(245) Castelletto, S.; Barbiero, M.; Charnley, M.; Boretti, A.; Gu, M. Imaging with Nanometer Resolution Using Optically Active Defects in Silicon Carbide. *Phys. Rev. Applied* **2020**, *14*, 034021.
(246) Budker, D.; Romalis, M. Optical magnetometry. *Nat. Phys.* **2007**, *3*, 227−234.
(247) Maze, J. R.; Stanwix, P. L.; Hodges, J. S.; Hong, S.; Taylor, J. M.; Cappellaro, P.; Jiang, L.; Dutt, M. V. G.; Togan, E.; Zibrov, A. S.; Yacoby, A.; Walsworth, R. L.; Lukin, M. D. Nanoscale magnetic sensing with an individual electronic spin in diamond. *Nature* **2008**, *455*, 644−647.
(248) Balasubramanian, G.; Chan, I. Y.; Kolesov, R.; Al-Hmoud, M.; Tisler, J.; Shin, C.; Kim, C.; Wojcik, A.; Hemmer, P. R.; Krueger, A.; Hanke, T.; Leitenstorfer, A.; Bratschitsch, R.; Jelezko, F.; Wrachtrup, J. Nanoscale imaging magnetometry with diamond spins under ambient conditions. *Nature* **2008**, *455*, 648−651.
(249) Rondin, L.; Tetienne, J.-P.; Hingant, T.; Roch, J.-F.; Maletinsky, P.; Jacques, V. Magnetometry with nitrogen-vacancy defects in diamond. *Rep. Prog. Phys.* **2014**, *77*, 056503.
(250) Abraham, J. B. S.; Gutgsell, C.; Todorovski, D.; Sperling, S.; Epstein, J. E.; Tien-Street, B. S.; Sweeney, T. M.; Wathen, J. J.; Pogue, E. A.; Brereton, P. G.; McQueen, T. M.; Frey, W.; Clader, B. D.; Osiander, R. Nanotesla Magnetometry with the Silicon Vacancy in Silicon Carbide. *Phys. Rev. Applied* **2021**, *15*, 064022.
(251) Li, Q.; et al. Room temperature coherent manipulation of single-spin qubits in silicon carbide with a high readout contrast. *Natl. Sci. Rev.* **2021**, nwab122.
(252) Sasaki, K.; Monnai, Y.; Saijo, S.; Fujita, R.; Watanabe, H.; Ishi-Hayase, J.; Itoh, K. M.; Abe, E. Broadband, large-area microwave antenna for optically detected magnetic resonance of nitrogen-vacancy centers in diamond. *Rev. Sci. Instrum.* **2016**, *87*, 053904.
(253) Ziem, F.; Garsi, M.; Fedder, H.; Wrachtrup, J. Quantitative nanoscale MRI with a wide field of view. *Sci. Rep.* **2019**, *9*, 12166.
(254) Hernández-Mínguez, A.; Poshakinskiy, A. V.; Hollenbach, M.; Santos, P. V.; Astakhov, G. V. Anisotropic Spin-Acoustic Resonance in Silicon Carbide at Room Temperature. *Phys. Rev. Lett.* **2020**, *125*, 107702.
(255) Simin, D.; Soltamov, V. A.; Poshakinskiy, A. V.; Anisimov, A. N.; Babunts, R. A.; Tolmachev, D. O.; Mokhov, E. N.; Trupke, M.; Tarasenko, S. A.; Sperlich, A.; Baranov, P. G.; Dyakonov, V.; Astakhov, G. V. All-Optical dc Nanotesla Magnetometry Using Silicon Vacancy Fine Structure in Isotopically Purified Silicon Carbide. *Phys. Rev. X* **2016**, *6*, 031014.
(256) Bourgeois, E.; Jarmola, A.; Siyushev, P.; Gulka, M.; Hruby, J.; Jelezko, F.; Budker, D.; Nesladek, M. Photoelectric detection of electron spin resonance of nitrogen-vacancy centres in diamond. *Nat. Commun.* **2015**, *6*, 8577.
(257) Gulka, M.; Bourgeois, E.; Hruby, J.; Siyushev, P.; Wachter, G.; Aumayr, F.; Hemmer, P. R.; Gali, A.; Jelezko, F.; Trupke, M.; Nesladek, M. Pulsed Photoelectric Coherent Manipulation and Detection of N-V Center Spins in Diamond. *Phys. Rev. Applied* **2017**, *7*, 044032.
(258) Siyushev, P.; Nesladek, M.; Bourgeois, E.; Gulka, M.; Hruby, J.; Yamamoto, T.; Trupke, M.; Teraji, T.; Isoya, J.; Jelezko, F. Photoelectrical imaging and coherent spin-state readout of single nitrogen-vacancy centers in diamond. *Science* **2019**, *363*, 728−731.
(259) Cochrane, C. J.; Blacksberg, J.; Anders, M. A.; Lenahan, P. M. Vectorized magnetometer for space applications using electrical readout of atomic scale defects in silicon carbide. *Sci. Rep.* **2016**, *6*, 37077.
(260) Falk, A. L.; Klimov, P. V.; Buckley, B. B.; Ivády, V.; Abrikosov, I. A.; Calusine, G.; Koehl, W. F.; Gali, A.; Awschalom, D. D. Electrically

https://doi.org/10.1021/acsphotonics.1c01775
ACS Photonics 2022, 9, 1434−1457

and Mechanically Tunable Electron Spins in Silicon Carbide Color Centers. *Phys. Rev. Lett.* **2014**, *112*, 187601.
(261) Wolfowicz, G.; Whiteley, S. J.; Awschalom, D. D. Electrometry by optical charge conversion of deep defects in 4H-SiC. *Proc. Natl. Acad. Sci. U. S. A.* **2018**, *115*, 7879−7883.
(262) Bonnin, O.; Guiot, E.; Schwarzenbach, W.; Picun, G. A greener SiC wafer with Smart Cut technology. *Compound Semiconductors* **2021**, *27*, 18.
(263) Margalit, N.; Xiang, C.; Bowers, S. M.; Bjorlin, A.; Blum, R.; Bowers, J. E. Perspective on the future of silicon photonics and electronics. *Appl. Phys. Lett.* **2021**, *118*, 220501.
(264) Nakadai, M.; Asano, T.; Noda, S. Electrically controlled on-demand photon transfer between high-Q photonic crystal nanocavities on a silicon chip. *Nat. Photonics* **2022**, *16*, 113.
(265) Borregaard, J.; Sørensen, A. S.; Lodahl, P. Quantum Networks with Deterministic Spin−Photon Interfaces. *Adv. Quantum Technol.* **2019**, *2*, 1800091.
(266) Peruzzo, A.; McClean, J.; Shadbolt, P.; Yung, M.-H.; Zhou, X.-Q.; Love, P. J.; Aspuru-Guzik, A.; O'brien, J. L. A variational eigenvalue solver on a photonic quantum processor. *Nat. Commun.* **2014**, *5*, 4213.
(267) Shadbolt, P. J.; Verde, M. R.; Peruzzo, A.; Politi, A.; Laing, A.; Lobino, M.; Matthews, J. C.; Thompson, M. G.; O'Brien, J. L. Generating, manipulating and measuring entanglement and mixture with a reconfigurable photonic circuit. *Nat. Photonics* **2012**, *6*, 45−49.
(268) Martini, F.; Gaggero, A.; Mattioli, F.; Leoni, R. Single photon detection with superconducting nanowires on crystalline silicon carbide. *Opt. Express* **2019**, *27*, 29669−29675.
(269) Thon, S. M.; Kim, H.; Bonato, C.; Gudat, J.; Hagemeier, J.; Petroff, P. M.; Bouwmeester, D. Independent electrical tuning of separated quantum dots in coupled photonic crystal cavities. *Appl. Phys. Lett.* **2011**, *99*, 161102.
(270) de Vries, M. O.; Sato, S.-i.; Ohshima, T.; Gibson, B. C.; Bluet, J.-M.; Castelletto, S.; Johnson, B. C.; Reineck, P. Fluorescent Silicon Carbide Nanoparticles. *Adv. Opt. Mater.* **2021**, *9*, 2100311.
(271) Economou, S. E.; Lindner, N.; Rudolph, T. Optically Generated 2-Dimensional Photonic Cluster State from Coupled Quantum Dots. *Phys. Rev. Lett.* **2010**, *105*, 093601.
(272) Webb, J. L.; Poulsen, A. F. L.; Staacke, R.; Meijer, J.; Berg-Sørensen, K.; Andersen, U. L.; Huck, A. Laser threshold magnetometry using green-light absorption by diamond nitrogen vacancies in an external cavity laser. *Phys. Rev. A* **2021**, *103*, 062603.
(273) Creedon, D. L.; Le Floch, J.-M.; Goryachev, M.; Farr, W. G.; Castelletto, S.; Tobar, M. E. Strong coupling between *P*1 diamond impurity centers and a three-dimensional lumped photonic microwave cavity. *Phys. Rev. B Condens. Matter.* **2015**, *91*, 140408.
(274) Le Floch, J.-M.; Delhote, N.; Aubourg, M.; Madrangeas, V.; Cros, D.; Castelletto, S.; Tobar, M. E. Towards achieving strong coupling in three-dimensional-cavity with solid state spin resonance. *J. Appl. Phys.* **2016**, *119*, 153901.
(275) Eisenach, E. R.; Barry, J. F.; O'Keeffe, M. F.; Schloss, J. M.; Steinecker, M. H.; Englund, D. R.; Braje, D. A. Cavity-enhanced microwave readout of a solid-state spin sensor. *Nat. Commun.* **2021**, *12*, 1−7.
(276) Reithmaier, J. P.; Sek, G.; Löffler, A.; Hofmann, C.; Kuhn, S.; Reitzenstein, S.; Keldysh, L.; Kulakovskii, V.; Reinecke, T.; Forchel, A. Strong coupling in a single quantum dot−semiconductor microcavity system. *Nature* **2004**, *432*, 197−200.
(277) Radulaski, M.; Fischer, K. A.; Vučković, J. Nonclassical light generation from iii−v and group-iv solid-state cavity quantum systems. *Adv. At. Mol. Opt.* **2017**, *66*, 111−179.
(278) Radulaski, M.; Fischer, K. A.; Lagoudakis, K. G.; Zhang, J. L.; Vučković, J. Photon blockade in two-emitter-cavity systems. *Phys. Rev. A* **2017**, *96*, 011801.
(279) Trivedi, R.; Radulaski, M.; Fischer, K.; Fan, S.; Vučković, J. *Photon blockade in the Tavis Cummings model.* https://meetings.aps.org/Meeting/MAR20/Session/C71.411, presented 03−02−2020, Bulletin of the American Physical Society, accessed 2022-03−09.
(280) Schmidt, S.; Blatter, G. Strong coupling theory for the Jaynes-Cummings-Hubbard model. *Phys. Rev. Lett.* **2009**, *103*, 086403.
(281) Hayward, A. L.; Martin, A. M.; Greentree, A. D. Fractional quantum hall physics in Jaynes-Cummings-Hubbard lattices. *Phys. Rev. Lett.* **2012**, *108*, 223602.
(282) Englund, D.; Majumdar, A.; Bajcsy, M.; Faraon, A.; Petroff, P.; Vučković, J. Ultrafast photon-photon interaction in a strongly coupled quantum dot-cavity system. *Phys. Rev. Lett.* **2012**, *108*, 093604.
(283) Cai, Y.; Roslund, J.; Ferrini, G.; Arzani, F.; Xu, X.; Fabre, C.; Treps, N. Multimode entanglement in reconfigurable graph states using optical frequency combs. *Nat. Commun.* **2017**, *8*, 1−9.

https://doi.org/10.1021/acsphotonics.1c01775
ACS Photonics 2022, 9, 1434−1457